

2003
54, 517



This is to certify that the
thesis entitled


STUDY OF A THICK COMPOSITE AND ALUMINUM
SINGLE-LAP BOLT JOINT EMPLOYING ORTHOTROPIC
PHOTOELASTICITY AND DIGITAL SPECKLE PATTERN
INTERFEROMETRY

presented by

Steven D. Thelander

has been accepted towards fulfillment
of the requirements for the

M.S. degree in Engineering Mechanics


Major Professor's Signature

June 13, 2003
Date

PLACE IN RETURN BOX to remove this checkout from your record.
TO AVOID FINES return on or before date due.
MAY BE RECALLED with earlier due date if requested.

DATE DUE	DATE DUE	DATE DUE
JUL 07 2017		

**STUDY OF A THICK COMPOSITE AND ALUMINUM SINGLE-LAP BOLT JOINT
EMPLOYING ORTHOTROPIC PHOTOELASTICITY AND DIGITAL SPECKLE
PATTERN INTERFEROMETRY**

By

Steven D. Thølander

A THESIS

**Submitted to
Michigan State University
in partial fulfillment of the requirements
for the degree of**

MASTER OF SCIENCE

Department of Mechanical Engineering

2003

ABSTRACT

STUDY OF A THICK COMPOSITE AND ALUMINUM SINGLE-LAP BOLT JOINT EMPLOYING ORTHOTROPIC PHOTOELASTICITY AND DIGITAL SPECKLE PATTERN INTERFEROMETRY

By

Steven D. Thelander

This thesis is part of a larger effort to research the strength of a single-lap, single-bolt joint between a thick Polymer Matrix Composite (PMC) and aluminum section that is representative of those to be employed on ARMY heavy-duty land vehicles. There has been little published research on the single lap bolted joint, which owes to the difficulty of such an analysis. The goal of this thesis was to contribute to the development of two experimental methods to analyze the stress distribution near the region around the bolt hole; then acquire results from those techniques to complement and verify the FEM stress predictions. The first method was an embedded polariscope orthotropic photoelastic stress analysis to study the contact stress distribution in the bearing plane of the composite between the bolt and bolthole. In order to model composite orthotropic behavior, a transparent birefringent orthotropic material was developed and characterized. The second experimental method was a Digital Speckle Pattern Interferometry (DSPI) surface strain analysis of the single-lap, bolted joint between composite and aluminum. Overall, the DSPI and photoelasticity results demonstrate that increasing bolt torque significantly decreases stress concentrations. Both methods need to be developed further in order to provide more information.

To my mother

ACKNOWLEDGMENTS

The author wishes to offer his sincerest appreciation and admiration to his graduate advisor, Dr. Gary Lee Cloud, for his guidance and support throughout this research. He also extends a dept of gratitude to David Hokens and Xu Ding for their technical expertise and countless hours of assistance. The author also would like to thank the other members of his committee, Dr. Tom Mase and Dr. Dahsin Liu, for their interest in this research. Last but not least, he thanks the secretaries of the Department of Mechanical Engineering for all of their help.

TABLE OF CONTENTS

LIST OF TABLES.....	vii
LIST OF FIGURES.....	viii
CHAPTER 1 - INTRODUCTION	1
1.1 Background Information.....	1
1.1.1 Polymer Matrix Composites	1
1.1.2 PMC Structures Joined with Mechanical Fasteners	3
1.2 Problem Description.....	7
1.3 Scope and Objectives	8
1.4 Literature Review	10
1.4.1 Choice of the Orthotropic Photoelasticity Method.....	10
1.4.2 Development of Transparent Birefringent Orthotropic Material	11
1.4.3 Development of Stress-Optic Law for Orthotropic Photoelasticity	17
1.4.4 Choice of Surface Strain/Stress Analysis Method	18
CHAPTER 2 – DEVELOPMENT AND CHARACTERIZATION OF ORTHOTROPIC	
PHOTOELASTIC MATERIAL	20
2.1 Considerations For Model Materials and Fabrication Techniques	20
2.2 Material Development.....	25
2.3 Fabrication of Calibration Specimens	34
2.4 Photoelastic Calibration of Material	36
2.5 Mechanical Characterization of Material	40

CHAPTER 3 – ORTHOTROPIC PHOTOELASTICITY ANALYSIS	45
3.1 Manufacture of the Specimen	45
3.2 Experimental Setup.....	48
3.3 Experimental Procedure	49
3.4 Results.....	49
3.5 Additional Experimental Notes.....	52
 CHAPTER 4 – SURFACE STRAIN ANALYSIS.....	 55
4.1 Brief Description of Digital Speckle Pattern Interferometry	55
4.1.1 Introduction	55
4.1.2 The Speckle Effect	55
4.1.3 A Simple In-plane Sensitive Setup for Displacement Measurement...	56
4.1.4 In-plane Phase Shifting DSPI.....	57
4.1.5 Strain Calculation Using Local Phase-unwrapping.....	59
4.2 The washer-nut.....	60
4.3 Manufacture of the Specimen	63
4.4 Experimental Setup.....	63
4.5 Experimental Procedure	66
4.6 Results.....	67
 CHAPTER 5 – CONCLUSIONS AND RECOMMENDATIONS.....	 71
 LIST OF REFERENCES	 79

LIST OF TABLES

Table 2.1 Epoxies evaluated for use as matrix in transparent composite.....	33
Table 2.2 Comparison of optical coefficients	39
Table 4.1 DSPI vs. RSG strain on pin connection	67

LIST OF FIGURES

Figure 1.1 Failure modes of a single bolt joint in tension.....	5
Figure 1.2 An exaggerated illustration of the effect of the eccentric loading generated by a single lap bolted joint	6
Figure 2.1 Photoelastic calibration setup.....	37
Figure 2.2 Coordinate system	37
Figure 2.3 Stress-birefringence curves for photoelastic characterization	39
Figure 2.4 Setup to determine E_1 , ν_{12} , ν_{13}	41
Figure 2.5 Setup to determine E_2 and E_3	42
Figure 2.6 Loading diagram to determine E_2	42
Figure 2.7 Loading diagram to determine E_3	42
Figure 2.8 Determination of E_1 , E_2 , and E_3	44
Figure 2.9 Determination of ν_{12} and ν_{13}	44
Figure 3.1 Specimen with transparent composite insert and embedded polariscope	46
Figure 3.2 Dimensioned photoelastic specimen	47
Figure 3.3 Orthotropic photoelasticity setup	48
Figure 3.4 Light field photoelasticity results for all clamping cases	51
Figure 3.5 Light field photoelasticity images for 25 In-lb bolt torque case	52
Figure 3.6 Coordinate system	53
Figure 3.7 Light field photoelasticity results.....	54
Figure 4.1 Simple in-plane speckle interferometer	56

Figure 4.2 Dual-beam illumination setup of phase shifting ESPI	58
Figure 4.3 Threading of Washer-Nut	62
Figure 4.4 Loading system for DSPI analysis.....	64
Figure 4.5 Diagram of composite specimen showing RSG locations	65
Figure 4.6 Phase map of initial area of interest for pin connection	66
Figure 4.7 Area of interest and strain line profile under washer-nut	66
Figure 4.8 DSPI phase change and strain map results	68
Figure 4.9 DSPI normalized strain line profile	69
Figure 5.1 Coordinate system	73

CHAPTER 1 - INTRODUCTION

1.1 BACKGROUND INFORMATION

1.1.1 POLYMER MATRIX COMPOSITES

Requirements for advanced materials from numerous industries led to the development of composite materials. A composite is a synergy of two or more distinct material constituents on a macroscopic level. Mechanical performance and properties of a composite are superior to those of the constituent materials acting alone. Composite materials have vastly enhanced product performance in aerospace, automotive, and recreational applications as a result of research and development efforts since the 1960s. This progress is primarily because the specific strength (strength-to-weight ratio) and specific stiffness (stiffness-to-weight ratio) of a composite can be superior to that of conventional metal alloys. Consequently, employing composites in lieu of metals can lead to a significant weight reduction in the structure, which directly results in fuel savings. Energy efficiency drives much of the development of composites in our energy conscious society.

Additional advantages of composites include good corrosion resistance, high fracture energy, and low thermal and electrical conductivity. In addition, the mechanical properties of a composite can be customized to meet specific design requirements. The shortcomings of composites include their relative inability to handle concentrated stress, the high cost of raw materials, and a more complex manufacturing process. Engineers need to be fully aware of the strengths and

limitations of composites in order to achieve optimal structural performance.

Composites will probably never entirely replace traditional materials like steel, but in many cases they are just what is needed. No doubt new uses will come about as the technology advances.

The most widely used type of composite material system is the polymer matrix composite (PMC). PMCs consist of two structurally complementary substances: reinforcing fibers such as glass or carbon and a matrix polymer such as epoxy, polyester, or urethane. Most materials are stiffer and stronger in the fibrous form than in any other shape. Accordingly, most of the composite strength is derived from fibers that are orientated in the load bearing direction; however, fibers alone cannot adequately support longitudinal compressive or transverse loads. Fibers are bound together in a structural unit with a matrix in order to utilize their directional strength, which also adds a small amount of needed ductility to the composite. A strong mechanical and chemical bond between the fiber and matrix is needed so that the matrix can transfer and distribute applied loads amongst the reinforcing fibers. To strengthen the bond, the fiber is coated with a sizing that increases the interfacial bond strength by acting as a coupling agent to provide a chemical link between the glass surface and matrix. Different sizings are available to match specific polymers. In addition to the coupling agent, to aid in processing, the sizing also contains film formers to hold filaments together, lubricants for abrasion resistance, as well as other additives such as antistats, emulsifiers, wetting agents, and antioxidants.

The amount of sizing on fiber ranges from 0.03% to 2% by weight. (Loewenstein 1993)

Mechanical properties such as strength, stiffness, and thermal expansion of PMCs depend largely on the type, quantity, and orientation of fibers. Clearly, the properties of a composite are derived in part by the properties of its individual constituents. Also, the weight or volume fraction of fiber-to-matrix will affect the mechanical properties of the composite. Furthermore, the directional strength of the reinforcement fibers make composite materials anisotropic or orthotropic, meaning that their mechanical properties vary with direction or depend on orientation. This flexibility allows engineers to tailor PMC properties to meet specific requirements by orienting the reinforcement. The exact stacking sequence of the fibers in a laminate composite can be designed to give different required mechanical properties in different directions. The composite can be made very strong in one direction by aligning the fibers that way, but it will be weaker in another direction where strength is not so important.

1.1.2 PMC STRUCTURES JOINED WITH MECHANICAL FASTENERS

One facet of composite structures that is of great interest involves joints that connect PMC members together. As in any structure made of conventional materials, a composite structure needs efficient, effective joints to transmit forces from one component to another. The strength of these connections is a critical factor that affects the overall structural performance.

PMC components are customarily joined with either adhesive bonding or mechanical fastening. Adhesive joints evenly transmit loads over a large area and consequently have minimal stress concentrations. Mechanically fastened joints on the other hand, tend to have a low structural efficiency that can impede their use in highly loaded primary structures. In bolted composite structures, stress concentrations develop around the holes, severely reducing the strength and fatigue life of the structure. However, many times bolted joints are needed for nondestructive component serviceability, for inspection, for replacement capability, or to give access to electronic components or mechanical subsystems in the structure interior.

Although there are many possible joint configurations, this thesis focuses on the study of single-lap, single-bolt joints of relatively thick plates. This simplified type of mechanical joint was chosen for study because it is a practical design of choice for many heavy-duty structural applications. Also, this study isolates as many variables as possible in order to study bolted joints more accurately.

Each joint must be properly engineered to be effective since failure of a single fastener can be destructive or even catastrophic. The failure modes of a single-lap, single-bolted joint in tension are shown in Figure 1.1.

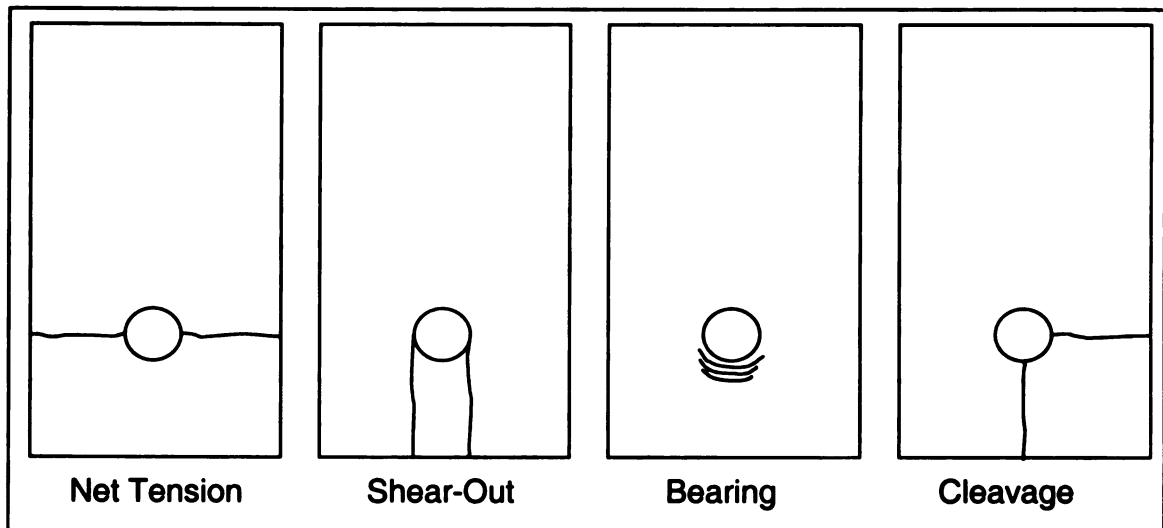


Figure 1.1 Failure modes of a single bolt joint in tension

The desired failure mode is bearing because it develops slowly, giving at least some warning before ultimate failure. The other modes usually occur prematurely at lower loads and can be catastrophic. One can design for bearing failure by adjusting stacking sequence and lay-up, and joint geometry (ratio of thickness, width, or edge distance to hole diameter).

Bearing failure is induced by high stress concentrations initiated by local contact at the hole-edge interface. The eccentric load path in a thick, single lap joint generates a bending moment. This bending moment produces a non-uniform bearing stress distribution through the thickness of the bolted region and subjects the bolt to a tensile stress as illustrated in Figure 1.2. Most of the previous analyses assumed that the bearing load was distributed sinusoidally over the projected contact area of the bolt because it is not known how the load is distributed to the bolthole, nor the relative deformations of the bolt and the components.

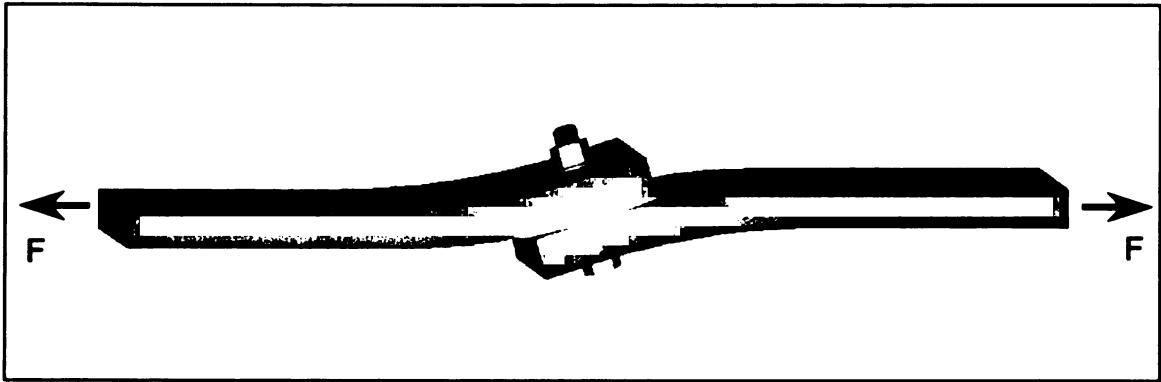


Figure 1.2 An exaggerated illustration of the effect of the eccentric loading generated by a single lap bolted joint

Although bolted joints in PMC exhibit bearing failure similar to that in metals, the mechanisms by which damage initiates and propagates is fundamentally different and complex. First, the anisotropy of a composite structure magnifies high stress concentrations at the bolthole. Also, the degradation of strength in PMCs caused by stress concentrations is amplified by an inability to deform plastically and heterogeneity. In isotropic materials, plasticity normally aids in reducing stress concentrations by redistributing the peak stresses. Unfortunately, PMCs do not exhibit this forgiving trait. In addition, the structural inhomogeneity of PMCs can lead to ply delamination. Polymer interlayers weaken the composite under crushing, compressive, and interlaminar shear stresses at the free edges of the bolthole. Delamination is a precursor to bearing failure (Ireman et al. 2000).

The clamping force provided by a tightened bolt can dramatically improve bearing strength (Cooper and Turvey 1995). The torque applied when the bolt is installed determines the clamping force. The main reason for an increase in bearing strength is that clamping causes a considerable part of the load to be transferred by friction between components, thereby reducing stress

concentrations at the hole-edge interface. Also, the clamping force prevents the delamination of plies and buckling of fibers in the highly stressed area. Despite the obvious advantages of studying the bolted joint, most of the studies performed have been limited to only pin joints. The reason for this anomaly seems to be because of the difficulty of analyzing the bolted joint.

1.2 PROBLEM DESCRIPTION

Uncertainties regarding the strength and failure modes of critical joints in PMC structures may, on one hand, lead to conservatively designed joints that eliminate some of the weight savings obtainable through the use of composites. On the other hand, under-designed joints may result in catastrophic in-service structure failure. Fortunately, a comprehensive structural analysis can provide an understanding of the factors controlling joint strength that ultimately produce optimal joint designs with consequent gains in efficiency. Engineers will be able to further push the envelope in exploiting composites to their full potential as a more thorough understanding of composite joint behavior is achieved. This understanding is advanced by the development of powerful analytical, numerical, and experimental techniques for structural analysis.

The U.S. Army Tank Automotive Research, Development and Engineering Center (TARDEC) is currently developing a heavy-duty land vehicle using thick composite and metal panels. A brief history behind the Army vehicle development can be found in Hodges (2000). To improve the overall structural design, TARDEC wanted to research the strength of a single-lap, single-fastener,

bolted joint between a thick PMC and metal section that is representative of those to be employed on Army heavy-duty land vehicles. TARDEC contracted this bolted joint study to Michigan State University.

Methods available for structural analysis include phenomenological mechanical tests that give the entire joint strength without the underlying failure mechanisms involved, stress analyses that give the locations and magnitudes of stress concentrations, and fracture mechanics analyses in which the micromechanisms of failure are considered.

A study by Hodges (2000) used destructive testing to evaluate the strength and mechanical properties of a single-lap, single-bolted joint between metal and composite. The test results demonstrated the potential to improve joint strength by increasing washer size and bolt preload.

This study aims to analyze the stress distribution near the region around the bolthole. The ultimate joint strength can be predicted with the stress distribution in conjunction with appropriate failure criteria. The results will be used as valuable input for structural design of heavy-duty, land vehicles. Furthermore, this study will add to the comprehensive knowledge base of orthotropic joint behavior.

1.3 SCOPE AND OBJECTIVES

The overall objective of this project is to analyze the three-dimensional stress state of a single-lap, single-fastener bolted joint between a thick composite

and metal section. This objective will be realized by means of both an accurate Finite Element Model (FEM) and experimental analysis.

The goal of this thesis is first to contribute to the development of two experimental methods, and then acquire results from those methods to complement and verify the FEM stress predictions. The first technique is 3-dimensional orthotropic photoelastic stress analysis in the bearing plane of the composite to study the non-uniform contact stress distribution between the bolt and bolthole. Since there has been very little done to employ orthotropic photoelasticity in three dimensions, as discussed in section 1.4.1, this research can be considered a pilot study. Orthotropic photoelasticity is discussed briefly in sections 1.4.1-1.4.3.

The second method is a surface strain analysis of the single-lap, bolted joint between composite and aluminum using Digital Speckle Pattern Interferometry (DSPI). DSPI is discussed in section 4.1. Even though the stress distribution is three dimensional, a surface strain analysis would provide useful information. Since DSPI has not been used to study the bolted joint, this research can be considered to be a pilot study.

The results from these analyses will be used to build a reliable FEM of the composite joint. The parameters of the FEM will be refined and tailored until its stress field correlates well with the experimentally derived stress field. A high correlation of FEM and experimental results will provide reasonable confidence in the results of the entire FEM.

1.4 LITERATURE REVIEW

1.4.1 CHOICE OF THE ORTHOTROPIC PHOTOELASTICITY METHOD

The development of fundamental photoelasticity theory, methods, and applications may be reviewed in Cloud (1995).

Macromechanical stress analysis can be conducted by means of orthotropic photoelasticity using transparent birefringent composites, which can be made to simulate the anisotropy of opaque PMCs (Daniel et al. 1984). Most of the studies on composites joints have been only two dimensional, largely because of the difficulty of a three-dimensional analysis. Prabhakaran (1982) as well as Hyer and Liu (1985) used two-dimensional orthotropic photoelasticity to study the stresses of pin-loaded PMC plates, which were at most 0.1 in thick. Although this method produced good fringes for thin specimens, the plate currently studied is thick enough that stresses will vary through the thickness. Accordingly, it will be necessary to perform a three-dimensional stress analysis to analyze photoelastic fringes through the edge of the composite. Furthermore, a pin-loaded plate may not adequately model the behavior of a single-lap, bolted joint.

There has been very little done to employ orthotropic photoelasticity in three dimensions. Chandrashekhara et al. (1977) explored the possibility of the application of the stress freezing technique to orthotropic composite models. It was concluded that it is possible to freeze stresses in specimens with low or high volume fiber fraction. However, it was found difficult to observe fringes in

specimens with more than about 10% fiber. Furthermore, this method is likely to lock stresses mostly in the matrix and not the reinforcement since the softening temperature of glass is significantly higher than the glass transition temperature of most resins.

Two other possible three-dimensional, photoelastic methods that have potential to be applied to orthotropic problems are the scattered light and embedded polariscope methods. While the scattered light method relies on model materials to not be optically perfect, composite models would scatter the light too much. The embedded polariscope method, developed by Tranmposch and Gerard (1961) and employed by Dally and Riley (1967) as well as Papirino and Becker (1966), may be the best solution for three dimensional, orthotropic photoelasticity. In this technique, the plane between the polarizer and analyzer may be isolated for photoelastic analysis. Tranmposch and Gerard showed that the presence of an embedded polariscope did not significantly alter the stress distribution of an epoxy specimen. However, it is not known how it will affect the stress distribution of a composite specimen because the polariscope will disrupt the orthotropic behavior. On the other hand, this method may provide a good approximation of the stresses at the composite/polarizer interface.

1.4.2 DEVELOPMENT OF TRANSPARENT BIREFRINGENT ORTHOTROPIC MATERIAL

Classic photoelasticity has long been used to effectively analyze the stresses in metals or other isotropic materials. However, standard photoelastic materials lack the fiber reinforcement needed to adequately model the orthotropic

behavior of PMCs. The following paragraphs review materials and processes used in studies to manufacture a transparent birefringent orthotropic material.

Horridge (1955) was the first known to attempt to fabricate a transparent birefringent composite for the purpose of orthotropic photoelasticity. He used glass satin weave cloth and Marco 28C resin (Scott Bader and Co.) that sufficiently matched the refractive index of the glass. Horridge achieved a .25" thick void free laminate with approximately 50% volume fiber by squeezing the air out with a rubber roller and later vacuum degassing the composite.

Hayashi (1962) used BHVT, EC-181, heat-cleaned silane-finished, satin weave and Rigolac 1553-L polyester resin. The resulting bi-directional model was about 10 plies and 8mm thick and contained 25% volume fiber.

Pih and Knight (1969) used a modified E-glass roving (W-1 glass by Owens-Corning Fiberglass, Inc. with a K895 finish) and Epon 815 Epoxy resin (Shell Chemical Co.) cured with triethylene triamine (TETA) and allyl glycidal ether mixed in a weight ratio of 100/12/2.5. They employed a wet-filament, winding technique that impregnated the roving with resin under vacuum. This process created void-free 0.125" thick 6" square plates that became translucent because the refractive indices were not well matched.

Sampson (1970) used HTS glass roving and DER 332 (Dow Epoxy Resin) cured with hexahydrophthalic anhydride (Dow Chemical Co.), both of which have a refractive index very close to 1.5490. The glass roving was first wound dry and then immersed in a resin bath under vacuum for two to three hours. This

technique yielded a 40% volume fiber-fraction transparent plate that produced good fringe patterns.

Grakh and Mozhanskaya (1971) used ED-6 epoxy resin with either A25 or A40 fiberglass cloth or SSA25 or SSA40 fiberglass net. First, they formed thin plates of resin and finely sanded them down to 0.3-0.5mm thick and placed one in a metal frame. Then they put a couple layers of glass fiber on the plate and soaked the fibers in epoxy glue, and placed on another plate. After that, they pressed out all the air bubbles and let cure at room temperature. They repeated this process until the composite had 28 layers of glass and was approximately 3mm thick. The thin plates of resin were used to reduce shrinkage and initial birefringence in the specimen. The resultant laminate had a 37% fiber volume fraction and was quite transparent and optically sensitive. Its mechanical anisotropy was quite high.

Dally and Prabhakaran (1971) used Style 7500 E-glass fabric with a Volan finish and Paraplex P444A Polyester (Rohm and Hass Co.) blended with 10 to 60 percent styrene monomer to match the refractive index of the glass. It was found that blending the polyester with 30 percent styrene cured with 0.5 percent benzoyl peroxide and 0.5 percent methyl ethyl ketone peroxide (MEKP) yields a resin with a refractive index of 1.548, which matches the E-glass refractive index. To make the composite, the glass was first soaked in a resin bath and then rolled between two sheets of Mylar to remove air. There was no need for degassing the composite in vacuum because the resin had a very low viscosity. Finally, the laminates were placed between heavy plates to prevent reentry of air and cured

in a platen press. This method made 10" X 12" laminates with 15 plies that were 0.075" thick.

Pipes and Rose (1974) used S-glass fibers (Owens Corning) and PL-2 epoxy resin (Photoelastic Incorporated). The glass was collimated by stretching fibers through an alignment comb and attaching fiber ends to the edges of the material mold with double sided adhesive tape. Four to ten layers of fiber were composed in this manner. Next, the mold was evacuated and epoxy resin was introduced into the mold. After curing, the composite plate was machined by a fly-cutting operation to provide flat parallel surfaces.

Chandrashekhara et al. (1977) used E-glass with Araldite CY-230 epoxy resin and Hardener HY-951 (CIBA of India) mixed in a weight ratio of 100/10. The fibers were arranged and stretched between the two edges of a frame to give a parallel array of fibers. The models were cast in vertical Perspex molds. Models were cast with 2, 4, and 6 percent fiber volume to study the variation of properties.

Agarwal and Chaturvedi (1978) used E-glass cloth and polyester resin with 0.4% cobalt octate and 1.0% MEKP. 5.0% dibutylphthalate and 2.0% divinyl benzene are added to match the refractive indexes of the resin to that of the glass. The refractive index of glass fibers has been quoted to be 1.549 ± 0.003 , but Agarwal notes that that value has not been found to be a very reliable one. The optimal chemical composition came after much trial and error. To fabricate the laminate, eight layers of glass cloth were placed on a Plexiglas mold, and a small quantity of resin was poured and brushed on each layer one by one. The

mold was then placed in a vacuum chamber to remove entrapped air. This process yielded a circular disc of 50mm diameter with a transmission ratio of 50%.

Prabhakaran (1980) developed a simple procedure to fabricate plates as large as 600 mm by 600 mm of arbitrary lay-up. A heavy steel or aluminum plate covered by a Mylar sheet provides the bottom and top molding and clamping surface. An aluminum frame fits snugly over the actual molding surface and has closely spaced screws on all four sides. The requisite number of layers of desired orientations is built up, pouring and spreading the resin between successive layers. Air bubbles are squeezed out with a rubber roller. The screws are then tightened to squeeze out excess resin.

Daniel et al. (1984) evaluated the following matrix materials to be used with Style 3733 E-glass fabric and S-910 finish (J.P. Stevens and Co.):

- Epon 815, cured with various amounts of amine hardeners, such as diethylene triamine (DETA) or TETA
- DER 332 epoxy cured with hexahydrophthalic anhydride (HHPA)
- Polyester resins such as Paraplex P444A, blended with styrene
- Marblette 658/558 epoxy resin
- CIBA 502 resin with Type 956 hardener

The Marblette epoxy turned out to be the most satisfactory. It cures at room temperature with a minimum amount of shrinkage and has a refractive index very close to that of E-glass (1.548). Sixteen layers of glass fiber were impregnated with resin, bagged, and cured in an autoclave at elevated temperature. This

technique produced a 0.095" thick water clear plate with a fiber volume fraction of over 50%.

Askadskii et al. (1987) modified the mechanical properties of polymers for use as stress freezing photoelastic models of composite structures. This method was accomplished by modifying the frequency of cross-linking to adjust the Mackian elasticity-modulus.

Agarwal et al. (1995) used E-glass fabric and sheet-grade polyester resin (Parikh Chemicals, Kampur), which has a refractive index of 1.538, close to that of the glass fibers (1.547). No additives were used to alter the optical properties of the resin. The composite plates were cast between two Mylar-lined plates and cured at room temperature for 24 hours and then post cured for 8 hours at 60°C. The cured plates exhibited an 8% fiber-volume fraction.

Zhang and Wang (1995) used both E-glass and Kevlar fibers with either 618-Epoxy resin or a bismaleimide copolymer resin. The epoxy resin was diglycidal ether of bisphenol A with 5% by weight 2-ethyl-4-methylimidazol as a curing agent. The BC resin was made by the copolymerization of 4,4'-phenylamide methyl type bismale imide (XU292A) with 2,2'-Diallylbisphenol A (XU292B) in a weight ratio of 100:87. Both resulted in a fiber-volume content of about 60% and very poor transparency. Instead of improving the transparency, they utilized the polarizing optical behavior of the composites in terms of transmitted polarized light intensity vs. azimuthal angle curve under the bright field of plane polariscopes. This technique was done with a Laser Microscopic Analyzer, which was built in-house.

Ravi (1997) used E-glass woven fabric and polyester blended with 5 to 60 percent styrene to match the refractive index of the glass. His findings duplicated those of Dally and Prabhakaran (1971), who found that blending the polyester with 30% styrene to match the refractive index of the glass (1.549) made for optimal transparency. There was no need for degassing the composite in vacuum because the resin had a very low viscosity. The resin was cured with 0.4% cobalt octate and 1% MEKP. The composite was cast in a mold made of rubber between two steel plates with Mylar lining. The finished composite plate had a 25% fiber volume fraction and achieved a transmission ratio of 87%.

Ravi et al. (2001) used a woven glass cloth weave (Harsh-Deep Industries, India) and sheet grade polyester resin (Parikh Chemicals, India), cured with 1% MEKP and 0.3% cobalt octate. They added 2% by weight divinyl benzene and 5% of dibutyl pthalate with the polyester to match the refractive index of glass. The composite plates are cast between two Mylar-lined Plexiglas sheets. Air bubbles are removed by vacuum. The completed composite plate had 33% fiber volume fraction and a maximum transmission ratio of 69.5% at 589nm.

1.4.3 DEVELOPMENT OF STRESS-OPTIC LAW FOR ORTHOTROPIC PHOTOELASTICITY

Ramesh and Tiwari (1993) reviewed the previous studies of orthotropic photoelastic theory. The authors used the existing works to develop stress-optic laws, strain-optic laws, and approximate strain-optic laws using uniform notation. It was determined that in order to characterize orthotropic model materials, an independent photoelastic constant is needed for all three directions.

Furthermore, they discussed the interpretation of isoclinics and the necessary steps to calibrate a birefringent orthotropic.

1.4.4 CHOICE OF SURFACE STRAIN/STRESS ANALYSIS METHOD

Ireman, Ranvik, and Eriksson (2000) used strain gages to determine the strain distribution in the vicinity of the bolthole. However, since strain gauges cannot accurately measure high strain gradients around a loaded hole because of finite gage lengths, a whole-field analysis seems to be a more appropriate approach. The following have simplified the bolted joint to a pin joint and employed a whole-field surface analysis.

Lu, Chen, and Lin (1993), as well as Rispler, Steven, and Tong (2000) used a photoelastic coating to evaluate the stress pattern of the pin joint. However, this method may not apply well to the bolted joint, because a tightened bolt would greatly affect the fringe pattern from the outset. Furthermore, the coating technique may not accurately reflect the specimen strain near the hole edge.

Herrera-Franco and Cloud (1992) along with Serabian and Anastasi (1991) used Moiré Interferometry to study the strain pattern of the pin joint. This method can provide high sensitivity results but requires the specimen to be smooth and can be arduous to set up. Additional information on the development of Moiré, methods, and applications may be reviewed in Cloud (1995).

Lanza Di Scalea et al. (1998) and Hong (1997) used Digital Speckle Pattern Interferometry (DSPI) to analyze the strain pattern of the pin joint. This method provides high sensitivity and is also the quickest and easiest method for whole field surface strain analysis. Also, the specimen need not be smooth for DSPI analysis. Section 4.1 briefly describes DSPI.

CHAPTER 2 – DEVELOPMENT AND CHARACTERIZATION OF ORTHOTROPIC PHOTOELASTIC MATERIAL

2.1 CONSIDERATIONS FOR MODEL MATERIALS AND FABRICATION TECHNIQUES

Primary characteristics necessary for a polymer matrix composite (PMC) model material are that it be orthotropic, birefringent, and transparent (Daniel et al. 1984). First, it needs the same type and orientation of fiber reinforcement as the PMC to be studied in order to adequately model the orthotropic behavior of a structure. Another requirement is that it needs to be photoelastically sensitive enough to generate adequate isochromatic fringe patterns. Furthermore, it needs to be transparent enough to view and record these fringe patterns under polarized light. The transparency of a material directly affects the quality of fringe patterns.

The transparency of PMC depends on matching the refractive indices of the constituent materials, the removal of entrapped air, wet-out of the fibers, fiber matrix compatibility, optical clarity of the constituent materials, and fiber content.

Although the constituent materials may be clear, a small difference between the refractive index of fiber and matrix will cause light to scatter at the fiber-matrix interface. The result is a translucent composite (Pih and Knight 1969). The change in refractive index at the interfaces causes light to deviate from its original straight-line path. The development of light refraction theory as well as several factors that affect the refractive index of glass and measurement methods for refractive index may be reviewed in Fanderlik (1983). Moreover, the

material interfaces are curved in glass fiber-matrix composites, which causes non-uniform deviation of light from different points on the interface of matrix and fiber. This deviation results in distortion of the light beam, smearing of sharp boundaries, and formation of a spectrum. As a consequence, closely spaced parallel lines viewed through the model will not appear distinct. (Agarwal and Chaturvedi 1978) Clearly, these effects are undesirable in photoelastic analysis as they reduce fringe visibility and sharpness. These effects can be minimized if not eliminated by matching the refractive indices of the constituent materials, so that the model is optically homogenous. Optical transparency can be achieved by matching the refractive index to within ± 0.002 (Olson, Day, and Stoffer 1992). An added difficulty is that the refractive index of the liquid resin is different from that of the cured resin. Hence, matching of the refractive indices has to be achieved when the resin is completely cured (Agarwal and Chaturvedi 1978).

Matching the refractive index can prove to be challenging because companies typically do not test for the refractive index of their production glasses given the nature of typical end-use performance needs. Customers are typically much more concerned about mechanical properties than non-mechanical properties of products. Furthermore, usual batching and melting operations will provide a seemingly broad range of refractive index, owing to normal variation in input of raw materials, which are extracted from various mines in many different countries (Allen 2002). These shifts however, generally take place over a relatively long period of time. The dependence of the refractive index upon the glass composition may be reviewed in Fanderlik (1983). This manufacturer's

lack of control over glass refractive index may explain why Agarwal and Chaturvedi (1978) did not find the glass fiber refractive index value quoted by the manufacturer to be reliable.

Another factor that could affect transparency is that the refractive index may vary along the fibers. A study by Kang et al. (1997) demonstrated that the refractive index of a glass fiber depends on its chemical composition and to some extent its thermal history (cooling rate). Consequently, the refractive index of the glass fiber will vary slightly with diameter since cooling rates varies inversely with the diameter. Even though the glass is pulled through dies of constant geometry, the fiber diameter depends on the glass flow rate through the nozzle and the velocity at which the fibers are drawn. Because these factors can change slightly with time, fibers can have a variation of diameter, which will cause a slight variation in the refractive index. Although this variance is in the third decimal point, it can limit the optical clarity of transparent composites.

Transparency is significantly affected by the entrapped air in the composite in the form of either bubbles or as a thin film at the fiber-matrix interface. Air bubbles can form when the resin is mixed or become entrapped in the glass cloth when the resin is poured. There are several methods to remove air from the composite. The larger bubbles can be pushed out with a roller after applying each layer of glass. The thin film of air is a result of either poor wet out or because of interface separation, which can occur if the fiber and matrix do not interact favorably. In order to achieve good wet out, the resin needs to penetrate through the fiber bundles and wet all the individual fibers (Agarwal and

Chaturvedi 1978). Two techniques to improve impregnation and proper wetting of fibers are employing a low viscosity resin as well as degassing the laminate in a vacuum. However, it may not be necessary to degas the composite if the matrix has a low enough viscosity (Dally and Prabhakaran 1971). Interface separation is when the polymer de-wets from the material, which forms thin voids and usually results in whitening in the sample (van Zanten et al. 1996). This behavior may be overcome with good fiber-matrix compatibility.

Another major limiting factor in the transparency of the composite is the clarity of the glass. E-glass fibers typically have small traces of impurities such as iron and chromium that contribute to a green color. Also, the sizing on the glass is tinted and likely has a different refractive index than that of the glass. Ravi (1997) tested to see whether removing the sizing would increase transparency in the composite. It was discovered that, to the naked eye, all the specimens appeared to be at the same transmission level; however, spectrophotometer results showed that removing the sizing actually decreased the light transmission. This behavior may be attributed to two factors. First, the fabric turns slightly yellow when heated to remove sizing, which causes some light to be absorbed. Secondly, removing the sizing may result in a poor fiber-matrix interface, which may impair the transparency.

It is possible that the poor transparency of E-glass may be overcome with the use of either fiber optic cables or optical grade glass. The filament made for fiber optic cables that are produced by Corning Glass or their licensees are extremely clear and void free and have a consistent refractive index. Fiber optic

filaments typically come on a spool and are not available in a fabric; however, they may be dry-wound over various metal frames in a filament winding machine to produce windings for various laminates, as Daniel et al. (1984) did with E-glass fibers. Also, fiber optic cables do not come with a sizing, which may or may not be desired. Using a different approach, Olson, Day, and Stoffer (1992) pulled glass fibers from a re-melted block of BK10 optical glass from Schott Glass Technologies to achieve the most transparent composite possible. However, since their matrix material, PMMA, is known to have a very low birefringence, the resultant laminate is not likely to prove useful in orthotropic photoelastic studies.

Another consideration is that the transparency of the composite will decrease with increasing fiber-matrix ratio because additional fiber increases the number of fiber-matrix interfaces. Also, an increased fiber-matrix ratio may lead to a decreased wet out of air.

Additional considerations for the matrix are pot life, cure time, and cure temperature. Ideally, the laminate should be laid up and degassed before the reaction initiates so that the resin cross-links throughout the entire laminate. Therefore, a short pot life limits the size of a composite that can be fabricated. Curing the matrix at an elevated temperature or curing it too quickly will introduce unwanted thermal stresses and create initial birefringence in the system. In addition, the initial birefringence may vary throughout the specimen. These stresses are created because of different thermal expansion rates of matrix and fiber (Grakh and Mozhanskaya 1971). Consequently, a slow cure at room

temperature is desired to ensure minimal residual stresses and initial birefringence in the final product.

2.2 MATERIAL DEVELOPMENT

A plain weave E-glass fabric style 3733 with S-910 finish manufactured by J.P. Stevens was chosen as the reinforcement. It is transparent, birefringent, and has a known index of refraction of 1.548. The glass has worked well in previous two-dimensional orthotropic photoelastic research (Daniel et al. 1981, Daniel et al. 1984, Doyle and Hyer 1985, Hyer and Liu 1985, and Liu 1990). However, the Marblette 658/558 epoxy resin used in those studies has not been manufactured since December 2000. Therefore, many epoxies have been obtained, and numerous composite samples have been fabricated and tested for their transparency and birefringence.

16-ply thick specimens were laid up in a 100ml plastic Nalgene beaker, approximately 1.5" in diameter. Each specimen transparency was subjectively rated (1=worst - 10=best), based on the resolution of lines seen through the specimen when placed over an EO Magnifier Quality Resolution Chart containing the 1951 USAF Test Pattern Groups 0-3 obtained from Edmund Industrial Optics.

The following paragraphs summarize the properties and chemistry of matrix resins tested in this study.

Measurements Group **PLM-9** Epoxy Resin is a specially formulated epoxy resin system for casting isotropic photoelastic models with section thickness up

to ½ in. When first cast, the composite was water clear. However, it was almost opaque after the composite specimen had cured because the refractive indices were matched before the resin began to gel and not when the resin was completely cured.

- Subjective Transparency = 1.5
- Cure Temp. = 120°F
- Refractive Index = ~1.6
- Resin/Hardener mix ratio = 100/7 by weight
- Chemical Composition:

Resin	%	Hardener	%
bisphenol a diglycidyl ether	>89.3	2,4,6-Tris (Dimethylamino/Methyl)	100
n-butyl glycidyl ether	2.7		
p-tertbutylphenyl glycidyl ether	0.8-8.0		
epichlorohydrin	Trace		
phenyl glycidyl ether	Trace		

Shell **EPON 828** is a clear, general-purpose epoxy resin, which has become a standard matrix used in fiber-reinforced composites. EPON 828 was easy to work with because of it has a very low viscosity, but the resultant laminate was opaque.

- Subjective Transparency = 1
- Cure Temp. = 175°F
- Refractive Index = 1.573
- Chemical Composition:

Resin	%	Hardener	pph
phenol, 4,4O - (1-methylethylidene) bis-polymer with (chloromethyl) oxirane	100	metaphenylenediamine	14

Derakane 441-400 and **Derakane 470-300** are epoxy vinyl ester resins with 33-weight percent styrene content, manufactured by the Dow Chemical

Company. These resins were chosen to attempt to replicate the method used by Dally and Prabhakaran (1971) and Ravi (1997), who blended polyester with 30 percent styrene to match the refractive index of glass. Both performed similar to the PLM-9, as they appeared water clear when cast but were opaque when the epoxy cured. Also, both needed to be cured quickly, and consequently had substantial initial stresses.

Derakane 441-400

- Subjective Transparency = 1
- Cure Temp. = 75°F
- Refractive Index = N/A
- Chemical Composition:

Resin	%	Hardener	pph
styrene monomer	33	mekp	1.50
vinyl ester resin	67	cobalt napthenate-6%	0.20
		dimethylaniline	0.05

Derakane 470-300

- Subjective Transparency = 1
- Cure Temp. = 75°F
- Refractive Index = N/A
- Chemical Composition:

Resin	%	Hardener	pph
styrene monomer	33	mekp	1.00
vinyl ester resin	67	cobalt napthenate-6%	0.20
		dimethylaniline	0.05

Sartomer **CN-151** is a clear Epoxy Methacrylate. The refractive index of the matrix closely matches that of the glass; however, CN-151 is extremely viscous and good wet-out was not possible. The resultant composite was quite opaque.

- Subjective Transparency = 0
- Cure Temp. = 75°F
- Refractive Index = 1.5500
- Chemical Composition:

Resin	%	Hardener	pph
bisphenol a epoxy methacrylate oligomer	100	mekp	1-2

Tra-Con Inc. **TRA-BOND 2115** is a clear, low viscosity epoxy formulation that cures at room temperature and is used in the fabrication of lasers. The resultant laminate was translucent.

- Subjective Transparency = 4
- Cure Temp. = 75°F
- Refractive Index = 1.55
- Resin/Hardener mix ratio = 100/30 by weight
- Chemical Composition:

Resin	%	Hardener	%
phenol, 4,4'-(1-methylethylidene) bispolymer with (chloromethyl) oxirane	80-100	1-prpanamine, 3,3'-(oxybis(2,1-ethanediylxy))bis	80-100
n-butyl glycidyl ether	<20		

Norland Products Inc. **NOA71** is an optically clear, liquid adhesive that will cure when exposed to long wavelength ultraviolet light. Although its refractive index of 1.56 is close to the glass, the end composite was semi-translucent. The adhesive cured very quickly under a lamp, and there may not have been enough to wet-out the glass.

- Subjective Transparency = 3
- Cure Temp. = 75°F
- Refractive Index = 1.56
- Chemical Composition:

Resin	%	Hardener	%
mercapto-ester	N/A	N/A	

Bicron **BC-600** Optical Cement is a clear, mid-viscosity epoxy resin formulated specifically for making optical joints with plastic scintillators. The finished laminate was fairly translucent.

- Subjective Transparency = 3
- Cure Temp. = 75°F
- Refractive Index = 1.56
- Resin/Hardener mix ratio = 100/28 by weight
- Chemical Composition:

Resin	%	Hardener	%
epoxy resin	>99	polyglycol diamine	N/A
modifiers	<1		

His Glassworks, Inc. **XTR-311** Epoxy Adhesive is an optically clear, low viscosity, high impact epoxy adhesive developed for bonding and small volume potting of plastic and glass optical fibers, lenses and prisms, LED displays, and other optical components. The completed composite was moderately translucent.

- Subjective Transparency = 4
- Cure Temp. = 75°F
- Refractive Index = 1.55
- Resin/Hardener mix ratio = 10/3 by weight
- Chemical Composition:

Resin	%	Hardener	%
phenol,4,4'-(1-methylethylidene) bispolymer with (chloromethyl) oxirane	80 -100	1-propanamine,3,3'-(oxybis(2,1-ethanedioxy))bis	80-100
n-butyl glycidyl ether	<20		

Star Technology Inc. **UVA4000** is a mid-viscosity epoxy used for potting and encapsulation. This two-part UV or room temperature curable epoxy has a

refractive index of 1.5470, which closely matches that of glass. However, the finished laminate was translucent.

- Subjective Transparency = 5
- Cure Temp. = 75°F
- Refractive Index = 1.5470
- Resin/Hardener mix ratio = 100/43 by weight
- Chemical Composition:

Resin	%	Hardener	%
epoxy resin	85-95	aliphatic amine	5-20
epoxy diluent	5-15	polyamine	20-50
photoinitiator	1-10	polymeric diluent	40-80

Epoxy Technology Inc. **EPO-TEK 301-2** is an optical grade epoxy that has excellent optical properties, a low viscosity, and a long pot life (8 hrs.) It is designed for optical applications such as bonding fiber optics (glass or plastic) and for optical filters. The end laminate was translucent.

- Subjective Transparency = 4
- Cure Temp. = 75°F
- Refractive Index = 1.564
- Resin/Hardener mix ratio = 100/35 by weight
- Chemical Composition:

Resin	%	Hardener	%
diglycidyl ether of bisphenol a	75-100	polyoxypropylenediamine	100

Epoxy Technology Inc. **EPO-TEK 302-3M** Optical Grade Epoxy is a two-component, clear epoxy that exhibits excellent optical properties and is recommended for bonding optical fibers into connectors, lens and prism bonding, and pigtailling to LEDs. The finished composite was opaque.

- Subjective Transparency = 1
- Cure Temp. = 75°F
- Refractive Index = 1.556
- Resin/Hardener mix ratio = 100/45 by weight
- Chemical Composition:

Resin	%	Hardener	%
bisphenol f	75-100	polyoxypropylenediamine	40-60
		aliphatic amine mixture	40-60

Epoxyset inc. Epoxibond **EB-106** and **EB-107** optical grade epoxies are designed to provide the good adhesion, transparency, and refractive index for many optical applications such as lenses laser windows, LEDs, prisms, and fiber optic applications. The specimen with EB-106 turned out translucent. In contrast EB-107 turned out to have the highest subjective transparency of all the evaluated matrices.

EB-106

- Subjective Transparency = 4
- Cure Temp. = 75°F
- Refractive Index = 1.56
- Resin/Hardener mix ratio = 100/30 by weight
- Chemical Composition:

Resin	%	Hardener	%
proprietary epoxy	N/A	proprietary hardener	N/A

EB-107

- Subjective Transparency = 9
- Cure Temp. = 75°F
- Refractive Index = 1.54
- Resin/Hardener mix ratio = 100/30 by weight
- Chemical Composition:

Resin	%	Hardener	%
proprietary epoxy	N/A	proprietary hardener	N/A

Epoxies, Etc... 20-3238 is a two-component, low-viscosity optical grade polymer epoxy system designed for L.E.D. encapsulating, fiber optic applications, and any potting application requiring the optimum clarity for inspection. The finished sample turned out somewhat translucent.

- Subjective Transparency = 2.5
- Cure Temp. = 75°F
- Refractive Index = 1.564
- Resin/Hardener mix ratio = 100/43 by weight
- Chemical Composition:

Resin	%	Hardener	%
epoxy resin produced by the condensation reaction of epichlorohydrin and bisphenol-a	>3	complex polyamine mixture	>1
residual epichlorohydrin	<.001		

Epoxies, Etc... 20-3302 is a two component, ultra-clear, epoxy system designed for L.E.D. encapsulating, fiber optics, and any potting or adhesive application requiring optimum clarity. It provides excellent optical transmission along with outstanding adhesion and electrical properties. This high purity grade polymer system is formulated with proprietary ultraviolet protectors to minimize yellowing of the cured epoxy. 20-3302 turned out remarkably transparent but was slightly less transparent than EB-107.

- Subjective Transparency = 8.5
- Cure Temp. = 75°F
- Refractive Index = 1.564
- Resin/Hardener mix ratio = 100/43 by weight
- Chemical Composition:

Resin	%	Hardener	%
epoxy resin produced by the condensation reaction of epichlorohydrin and bisphenol-a	>3	complex polyamine mixture	>1
residual epichlorohydrin	<.001		

Table 2.1 summarizes the evaluated matrixes in order of refractive index.

All matrix material property data including refractive index were obtained from individual manufacturers. Each company may use a different method to test for refractive index; as a consequence there may be slight errors in the data.

Epoxy	Refractive Index	Subjective Transparency (1=worst-10=best)	Viscosity @ 75°F (cps)	Pot Life (Min.)	Approx. Cure Time (Hours)
Derakane 441-400	N/A	1	400	50	12
Derakane 470-300	N/A	1	300	50	12
EB-107	1.54	9	300	30	48
20-3238	1.5403	2.5	500	45	18
UVA4000	1.5470	5	610	70	24
CN-151	1.5500	1	2190	N/A	8
XTR-311	1.55	4	500	60	24
TRA-BOND 2115	1.55	3	250	120	24
EPO-TEK 302-3M	1.5560	1	800	90	24
NOA71	1.56	3	200	N/A	0.5
BC-600	1.56	3	800	30	24
EB-106	1.56	4	150	45	48
20-3302	1.564	8.5	500	45	36
EPO-TEK 301-2	1.564	4	450	480	48
EPON 828	1.573	1	150	N/A	4
PLM-9	~1.6	1.5	N/A	N/A	48

Table 2.1 Epoxies evaluated for use as matrix in transparent composite

The next step was to see which of the two most transparent specimens, EB-107 and 20-3302, produced the best fringes though the thickness of the material. One-quarter-inch thick sections were cut out and then polished. The two sections were viewed in a polariscope while loaded in three-point bending. Even though the EB-106 specimen is slightly more transparent, the 20-3302 sample generated sharper fringes, possibly because the 20-3302 may be more birefringent.

Therefore, the 20-3302 is the optimal matrix material for the E-glass fibers chosen. The 20-3302 might not work as well with other E-glass because there is a broad range of glass compositions that meet the definition of E-glass.

2.3 FABRICATION OF CALIBRATION SPECIMENS

Since the orthotropic photoelasticity material was new, it was necessary to fabricate uniaxial test specimens to generate the data required to establish the stress-optic coefficients and mechanical properties. The first step was to construct an open-faced mold from $\frac{1}{2}$ " thick melamine. The inside dimensions of the mold were 7" x 3" x 1". Since the laminates edges will be very matrix rich, it is necessary to make the mold approximately $\frac{3}{8}$ " larger on all sides than the finished plate needs to be. All inside corners of the mold were sealed with DAP Kitchen and Bath 100% Silicone Sealant. No mold release was used. A guillotine paper cutter was used to cut $14 \pm 90^\circ$ and $13 \pm 45^\circ$ fiberglass layers to loosely fit the mold. The guillotine was key so that the weave was not altered,

and it allowed straight fiberglass rectangles to be cut out with ease. The next step was to lay-up the fiberglass and resin in the mold. To begin, the 30-3302 epoxy and hardener was thoroughly mixed. Next, a wooden tongue depressor was dipped in the resin and swirled around the mold, just enough to wet the bottom of the mold. Then one layer of $\pm 90^\circ$ fiberglass was placed over the resin. Afterward, the resin was evenly spread around with a small glass vial. It was important to use as little resin as possible and still wet-out the fibers to avoid air bubbles becoming trapped. Next, one layer of $\pm 45^\circ$ fiberglass was placed over the $\pm 90^\circ$ fiberglass, followed by a small quantity of resin. The addition of alternating fiberglass layers and resin and removal of bubbles continued until the laminate had 27 layers and was approximately $\frac{1}{4}$ " thick. It was important to finish the lay-up of plies within the pot life of 45 minutes.

The composite was degassed once lay-up was completed and as much air as possible was removed with the vial. First, a layer of $\frac{1}{4}$ " hardware cloth was set just above the fiberglass to prevent shifting of plies while in vacuum. Then a -29 in. Hg vacuum was drawn on the mold for approximately one hour at room temperature in a VW12 Scientific Inc. 1410 Vacuum Oven coupled to a Model DD50 Precision Vacuum Pump. Then the mold was removed from the vacuum chamber, and the hardware cloth was lifted off of the laminate. At that time additional resin was spread on the composite. Next, the mold was placed on a level surface and cured at room temperature for approximately 36 hours.

After the composite plate fully cured, it was released by dismantling the mold. Next, a band saw was used to cut the plate into three- $\frac{3}{8}$ " and two- $\frac{1}{4}$ " wide tensile specimens. Subsequently, the specimens were polished with 320, 600, and then 1200 grit paper in a Struers Abramin Microprocessor controlled bench top machine for automatic grinding and polishing. A small amount of resin was added to each side to aid in transparency.

2.4 PHOTOELASTIC CALIBRATION OF MATERIAL

Figure 2.1 shows the diffused light polariscope and load frame designed by J.T. Pindera and G.L. Cloud (Cloud 1995) used to photoelastically calibrate the material. This setup used a $\lambda=589\text{nm}$ sodium lamp. The specimen was mounted in grips designed that allow rotation to reduce bending as shown in Figure 2.1.

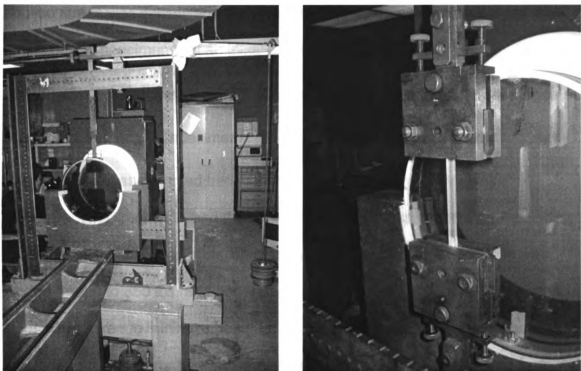


Figure 2.1 Photoelastic calibration setup

Figure 2.2 defines the composite plate coordinate system that shall be used throughout this thesis.

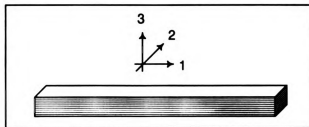


Figure 2.2 Coordinate system

The stress-optic coefficient, F_3 was determined in tension utilizing the Tardy method of goniometric compensation (Cloud 1995), with one of the $\frac{3}{8}$ " X $\frac{1}{4}$ " uniaxial test specimens. The specimen was loaded from 0 to 450 lbs. and generated a maximum of 2.75 fringes. The applied stress vs. fringe order is plotted in Figure 2.3. The slope of this plot is $F_3 = 504.2$ psi-in./fringe. The

applied stress was calculated using force divided by cross-sectional area. Also, the unloaded specimen had an initial birefringence of 0.083.

F_2 was determined by direct observation of whole and half order fringes with one of the $\frac{1}{4}$ " x $\frac{1}{4}$ " specimens. The Tardy method of goniometric compensation was not used because the laminate is significantly less transparent in Direction 2, and the background brightness varied as the polarizer rotated, which made determination of fringe very difficult. The specimen was loaded from 0 to 350 lbs. and generated a maximum of 3.5 fringes. Although steps were taken to minimize bending, the load system was still misaligned. As a result, for each fringe order there was a single vertical fringe that moved from right to left through the specimen. Fringe orders were recorded when the fringe was in the middle of the specimen. The applied stress vs. fringe order is plotted in Figure 2.3. The slope of this plot is $F_2 = 415.3$ psi-in./fringe. The Tardy method of goniometric compensation method was used to determine an initial birefringence of 0.166.

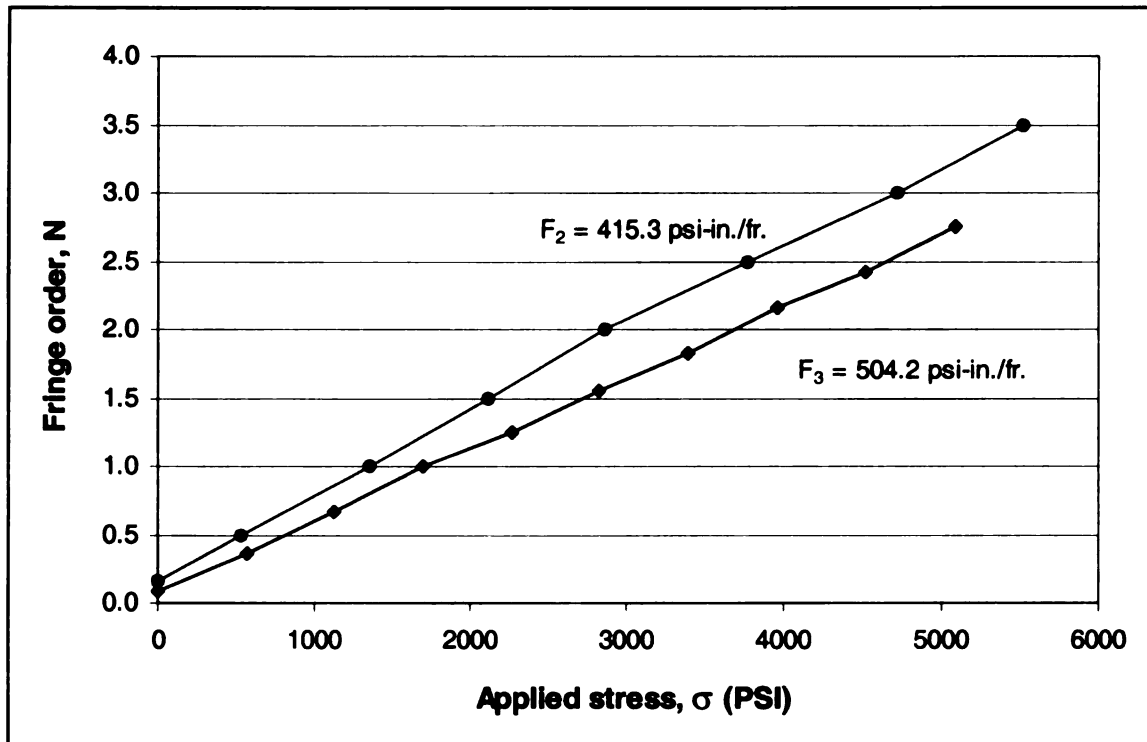


Figure 2.3 Stress-birefringence curves for photoelastic characterization

The stress-optic coefficients established are comparable to numerous other orthotropic photoelasticity studies, as seen in Table 2.2. Because each study used different notation, orientation, and ply lay-up, only the range of all stress-optic coefficients reported is displayed.

Study	Stress-optic coefficient range (psi-in./fr.)	Initial birefringence range (fringe)
current research	415-504	0.083-0.166
Sampson (1970)	220-550	
Dally and Prabhakaran (1971)	955	0.15
Pipes and Dalley (1973)	596	0.15
Pipes and Rose (1974)	40-100	
Agarwal and Chaturvedi (1978)	261-618	0.25
Daniel et al. (1984)	191-417	0.43-0.45

Table 2.2 Comparison of optical coefficients

2.5 MECHANICAL CHARACTERIZATION OF MATERIAL

To determine modulus of elasticity E_1 , and the Poisson's ratios ν_{12} and ν_{13} , another one of the $\frac{3}{8}$ " x $\frac{1}{4}$ " uniaxial test specimens was setup in the same load frame used for photoelastic calibration as shown in Figure 2.4. Also shown in Figure 2.4 is the placement and orientation of Micro-Measurements WA-06-030WR-120 resistance strain gage rosettes bonded on all four sides of the specimen. The gages were connected to a Measurements Group SB-10 Switch & Balance Unit coupled to a Measurements Group P-3500 Strain Indicator setup in half-bridge configuration with a temperature compensation gage mounted on an unloaded specimen. The gages were named according to the side on which they are mounted and their orientation, i.e. A_1 refers to the gage on side A in Direction 1.

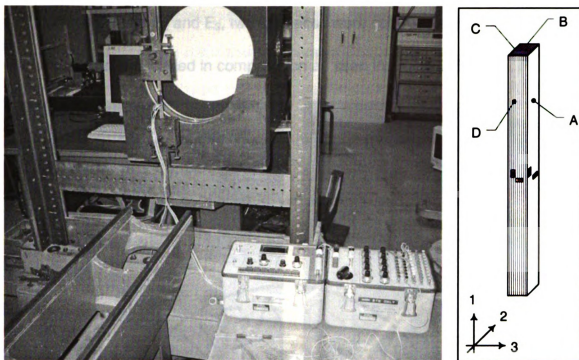


Figure 2.4 Setup to determine E_1 , ν_{12} , ν_{13}

To minimize any effect of bending because of the misalignment of loading fixture, the load setup was adjusted until gages A_1 , B_1 , C_1 , and D_1 gave strains within 10% of each other. Small polarizer and analyzer sheets were also used to check for bending by observing fringes. The tensile specimen was loaded from 0 to 350 lbs. To determine E_1 , the average of gages A_1 , B_1 , C_1 , and D_1 was plotted vs. applied stress as shown in Figure 2.8 on page 44. To determine ν_{13} , the average of gages B_1 and D_1 are plotted vs. the average of gages B_3 and D_3 as shown in Figure 2.9 on page 44. Likewise, to determine ν_{12} , the average of gages A_1 and C_1 were plotted vs. the average of gages A_2 and C_2 as shown in Figure 2.9 on page 44.

To determine E_2 and E_3 , two $\frac{3}{8}$ " pieces were cut from a $\frac{3}{8}$ " x $\frac{1}{4}$ " uniaxial test specimens and loaded in compression as seen in Figure 2.5.

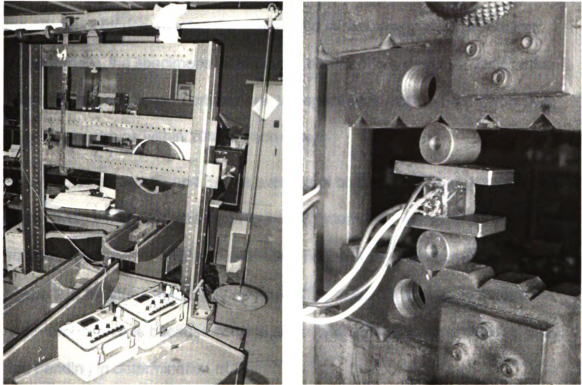


Figure 2.5 Setup to determine E_2 and E_3

Two Micro-Measurements EA-13-120LZ-120 single-element resistance strain gages were mounted on both faces of each specimen. Figure 2.6 and Figure 2.7 illustrates the loading direction and fiber orientation used to determine E_2 and E_3 respectively.



Figure 2.6 Loading diagram to determine E_2

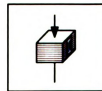


Figure 2.7 Loading diagram to determine E_3

Both gages were connected to separate P-3500 Strain Indicators setup in half-bridge configuration with a temperature compensation gage mounted on an unloaded specimen. It should be noted that it is not known how edge effects and the effects of friction affected the results. To minimize any effect of loading misalignment, the specimens were placed between two steel cylinders, which allowed small rotations. Furthermore, the specimens were adjusted until both gages gave strains within 10% of each other.

To determine E_2 and E_3 , the average of both E_2 and E_3 gages were plotted respectively vs. applied stress in Figure 2.8. Ideally, E_1 will equal E_2 if there is an equivalent number of $\pm 90^\circ$ and $\pm 45^\circ$ fibers in the specimen. However, as seen in Figure 2.8, E_1 differs from E_2 by approximately 15%. This difference does not seem unreasonable because of edge and friction effects in determination of E_2 , and bending in determination of E_1 .

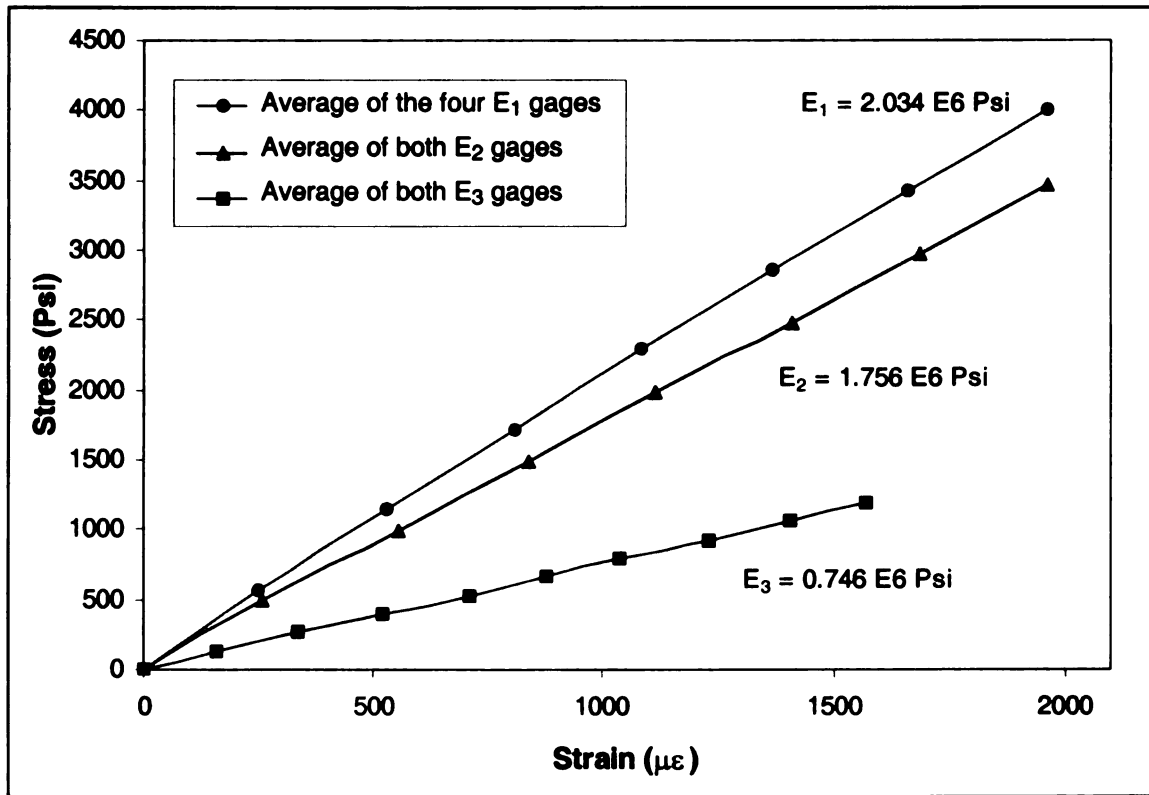


Figure 2.8 Determination of E_1 , E_2 , and E_3

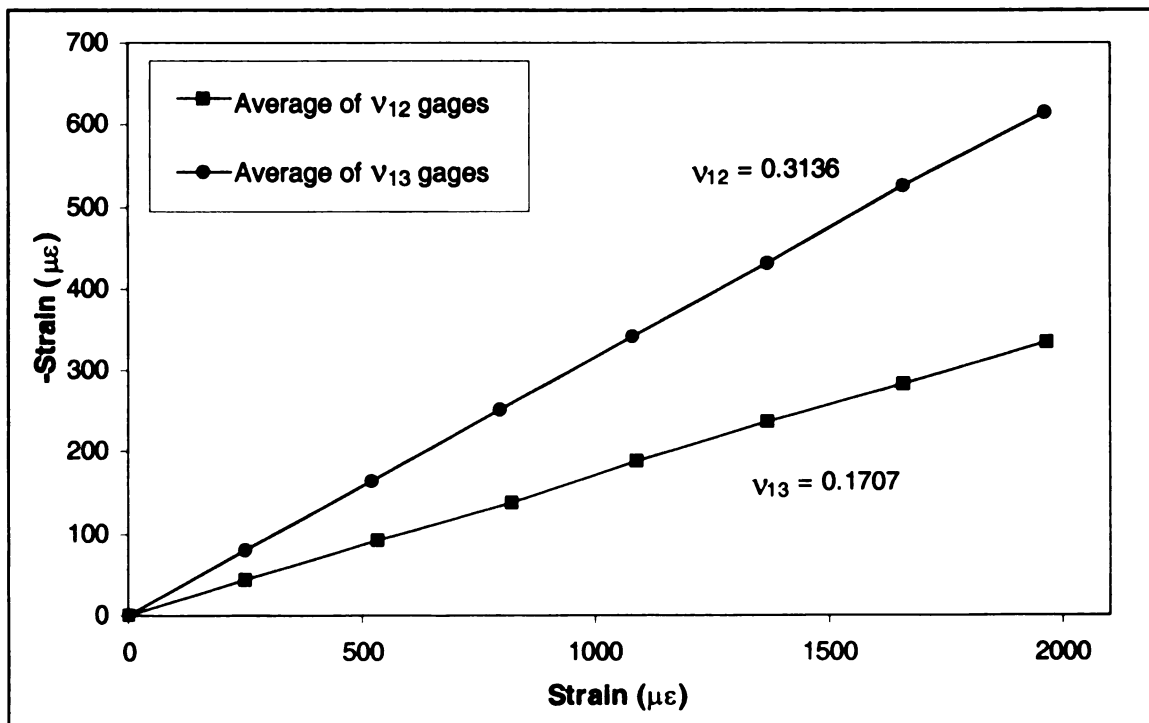


Figure 2.9 Determination of ν_{12} and ν_{13}

CHAPTER 3 – ORTHOTROPIC PHOTOELASTICITY ANALYSIS

3.1 MANUFACTURE OF THE SPECIMEN

Ideally, the transparent specimen would be comprised entirely of the orthotropic photoelastic material. Although the material developed is transparent enough for a two-dimensional analysis of a ½" thick plate, the material was not transparent enough for three-dimensional work with an embedded polariscope to analyze fringe patterns through four inches of material. A two-dimensional analysis would not be very useful since the stresses are expected to vary through the thickness. A small 1" wide specimen with an embedded polariscope was not transparent enough to generate adequate fringes; consequently, a composite specimen 4-inches wide was not fabricated. As an alternative, the photoelasticity specimen will only contain a composite slice in the area to be analyzed. The rest of the plate will be a sheet of LEXAN 9034 transparent polycarbonate sheet from GE Structured Products as shown in Figure 3.1. This model is not the most accurate possible since the stresses in the composite slice are affected by stress elsewhere in the plate, which is an isotropic plastic. Furthermore, an isotropic plastic plate most likely would distribute stress much differently than an orthotropic one. Regardless, this setup may be a better approximation than an entirely isotropic model.

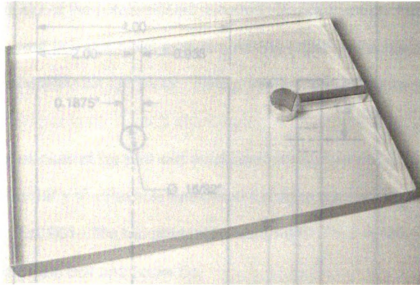


Figure 3.1 Specimen with transparent composite insert and embedded polariscope

To ensure a bearing failure mode was analyzed, the specimen edge-to-hole distance ratio is three, pitch-to-hole distance ratio is eight, and the diameter-to-thickness ratio is one.

To manufacture the specimen, the polycarbonate plate was first cut in a band saw and then milled down to 6" x 4". A 15/32" hole was drilled 1.5" from the end as shown in Figure 3.2. A 0.1875" wide slice below the bolthole was removed with a band saw, and then the inside plate walls were smoothed over with a fine file. The plate edges were polished with 600, 1200, and then 4000 grit paper in a Struers Abramin polisher.

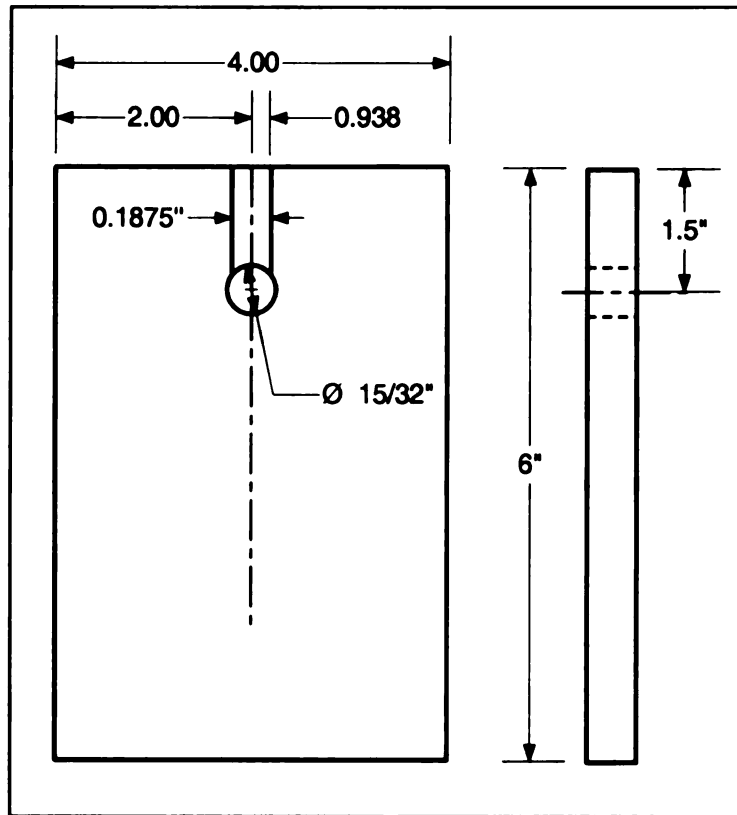


Figure 3.2 Dimensioned photoelastic specimen

To fabricate the composite slice, an open faced mold with inside dimensions of 2" x 2" x 1" was constructed out of ½" thick melamine. The specimen block was laid up in a manner similar to that used for the calibration specimen in Section 2.2, except that it had a thickness of ½" and 54 layers. Then a 0.25" slice was cut from the composite block with a band saw and polished with 300 and 600 grit paper until the slice was able to easily slide in and out of the space in between the polarizer and analyzer in the polycarbonate plate. The finished laminate slice was 0.154" thick.

The polarizer and analyzer with $\lambda/4$ plate were cut to size from a sheet of Polaroid filter medium, CP-01P from International Polarizer, Inc. The polarizer and analyzer were bonded to the composite slice, and then that sandwich was

bonded in the slot of the polycarbonate sheet with 30-3302 epoxy. Next, the excess epoxy and polarizer sheet were removed by polishing the specimen surface with 600 and 1200 grit paper. Finally, the hole was bored out to $.500'' \pm 0.0005$.

The other plate of the joint was machined from a sheet of $\frac{1}{2}''$ thick 2024-T4 aluminum to $10'' \times 4''$. The hole was drilled 1.5'' from the plate end and reamed to $0.5'' \pm 0.001$. The two plates were connected with a $\frac{1}{4}''$ -20 shoulder bolt from Mid-States Bolt and Screw Co.

3.2 EXPERIMENTAL SETUP

The joint was mounted in the diffused light polariscope and load frame used in the photoelastic calibration described in Section 2.4. The setup is shown in Figure 3.3.

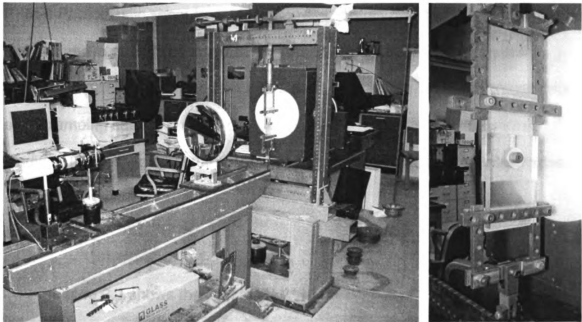


Figure 3.3 Orthotropic photoelasticity setup

The free ends of the polycarbonate and aluminum plates were clamped between two 1" wide steel beams. A field lens with a 1-meter focal length was placed in front of the specimen. A COHU Solid State CCD (charge-coupled device) Camera Model 4812-2000 coupled with a Nikon Coligon Zoom Lens 1:6.3 $f=95\text{mm}-205\text{mm}$ was placed at the field lens focal length. The images were captured with a LabVIEW (National Instruments Corp.) program, developed by Xu Ding.

3.3 EXPERIMENTAL PROCEDURE

The joint was tested for three different clamping cases: pin joint, finger tightened, and 25 in-lb bolt torque. It was not possible to test at higher clamping forces because of insufficient bonding shear strength between the polycarbonate, polarizers, and composite slice. Previous experience with similar plates made of PSM-9 Photoelastic sheet from Measurements Group failed when the bolt was torqued above 40 in-lb because of insufficient bonding shear strength at the embedded polariscope. The joint was loaded from 0-80lb in 20lb increments for each clamping case in order to compare the results with the same external loading. Images were captured after the specimen was loaded for five minutes.

3.4 RESULTS

Figure 3.4 shows the light field photoelasticity results for all the clamping cases. At 0 lb load the pin connection and finger-tighten cases appear to have

minimal fringes, whereas the unloaded 25 in-lb case shows that the torque clamping force alone caused a large evenly distributed fringe area. As loading is increased from 0-80 lb for the pin connection and finger-tightened case, a stress concentration develops in the corner of the bolt and shearing plane; however, the finger-tighten case stress concentration is significantly smaller. As loading is increased for the 25 in-lb case from 0-80 lb, no significant stress concentrations can be seen, as the fringe pattern is virtually unaffected with increasing loads. Overall, it can be seen that increasing the clamping force decreases the stress concentration at the shearing corner. This pattern was as expected because the clamping of a tightened bolt causes a considerable part of the applied load to be transferred by friction between components, thereby reducing stress concentrations at the hole-edge interface.

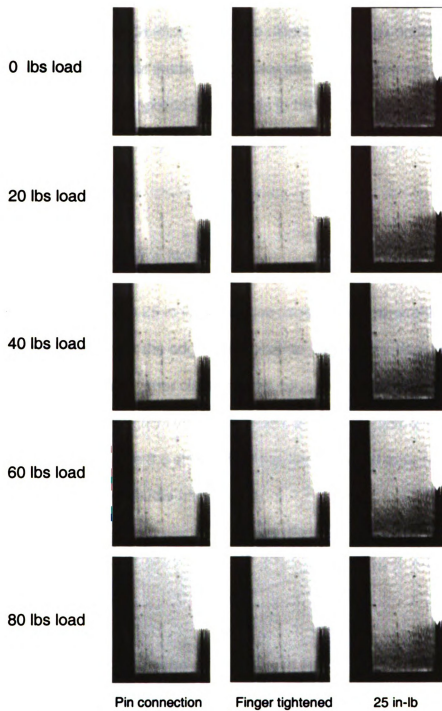


Figure 3.4 Light field photoelasticity results for all clamping cases

The joint failed when the polarizer de-bonded from the polycarbonate plate while in loaded pin connection after testing the different loading conditions up to 80 lbs. It was determined that the bonding shear strength between polarizers, polycarbonate plate, and composite slice needs to be significantly improved before testing continues, as the joint is likely to see loads of 10,000-20,000 lbs in service (Hodges 2000).

3.5 ADDITIONAL EXPERIMENTAL NOTES

It was noticed that the 25 in-lb bolt torque case initially generated a fairly distinct horizontal fringe near the edge of the washer through the thickness of the plate. However, immediately after clamping, the fringe expanded toward the bolt under the washer. After roughly five minutes the large evenly distributed fringe area remained stable. Figure 3.5 shows the analyzed area just after torque was applied, and the area five minutes after torque.

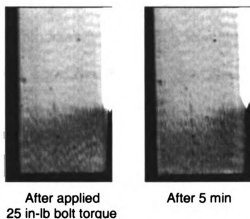


Figure 3.5 Light field photoelasticity images for 25 In-lb bolt torque case

To further investigate this time effect, a pilot test was conducted with two of the calibration specimens manufactured for the photoelastic calibration that was discussed in Section 2.4. This experiment used the polariscope described in Section 2.4, and a small screw-operated loading frame to load the specimens in four point bending. Specimen A, which is $\frac{1}{4}$ " x $\frac{1}{4}$ " x 7", was setup in the load frame so that fringes could be viewed in Direction 2 as defined in Figure 3.6. Specimen B, which is $\frac{3}{8}$ " x $\frac{1}{4}$ " x 7", was set up in the load frame so that fringes could be viewed in Direction 3.

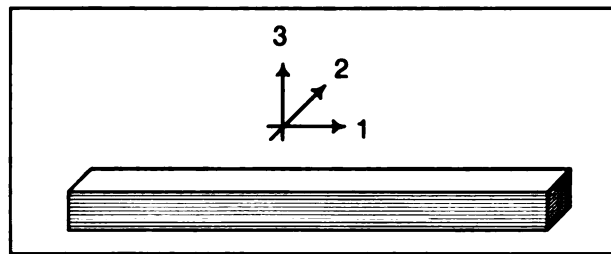


Figure 3.6 Coordinate system

Figure 3.7 shows specimens A and B just after load was applied, and after five minutes of constant deformation. After load, specimen A initially generated two fairly distinct fringes that immediately began to widen and shift towards the beam edge. Likewise, after load, specimen B initially generated 4 distinct fringes that immediately began to shift towards the beam edges. After five minutes the fringe order of specimen B was cut roughly in half.

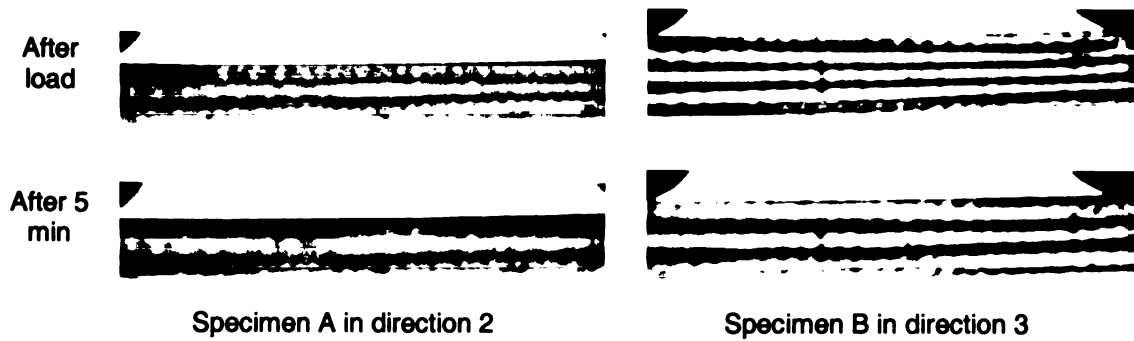


Figure 3.7 Light field photoelasticity results

One possible explanation for this behavior is that a relaxation of birefringence in the composite may be related to a relief of stress in the epoxy matrix. After load is applied the matrix will creep at a much faster rate than the glass fibers, which may cause some forces originally borne by the matrix to be transferred over time to the fibers. Glass is known to have significantly less birefringence sensitivity than epoxy; so, as load is transferred from epoxy to glass fiber, the birefringence will decrease in the epoxy significantly more than it will increase in the glass, resulting in a reduced fringe order. This phenomenon is not well understood or documented and needs to be researched further.

CHAPTER 4 – SURFACE STRAIN ANALYSIS

4.1 BRIEF DESCRIPTION OF DIGITAL SPECKLE PATTERN INTERFEROMETRY

(DSPI) technique used to analyze the surface strain field of the joint. DSPI is a precise non-contact real-time method to quickly measure whole field surface displacements and strain fields. It can also be used for nondestructive evaluation (NDE). In this research, a dual-beam-illumination speckle interferometer is used to measure the in-plane strain in the vicinity of the specimen bolt hole. The following information was drawn from Cloud (1995), Hong (1997), Jones and Wykes (1989), and Lanza Di Scalea (1996), who present a more detailed development of DSPI theory, methods, and applications.

4.1.2 THE SPECKLE EFFECT

When a laser illuminates a surface that is minutely rough (on the order of the laser wavelength), each point on the surface acts as a point source of a scattered light spherical wave front. Interference of the coherent waves arriving at a receiving point will result in a speckle ranging from completely dark to fully bright. Each neighboring point, which is illuminated by different waves, will most likely give a much different brightness. The variation in resultant irradiance across the illuminated area appears as grainy structures on the surface, which is known as the speckle effect or laser speckle.

4.1.3 A SIMPLE IN-PLANE SENSITIVE SETUP FOR DISPLACEMENT MEASUREMENT

A typical in-plane dual-beam illumination speckle interferometer that combines two coherent speckle patterns to make a new speckle pattern is shown in Figure 4.1. Two beams inclined at equal and opposite angles, θ , from the object surface normal illuminate the object, which lies in the xy -plane.

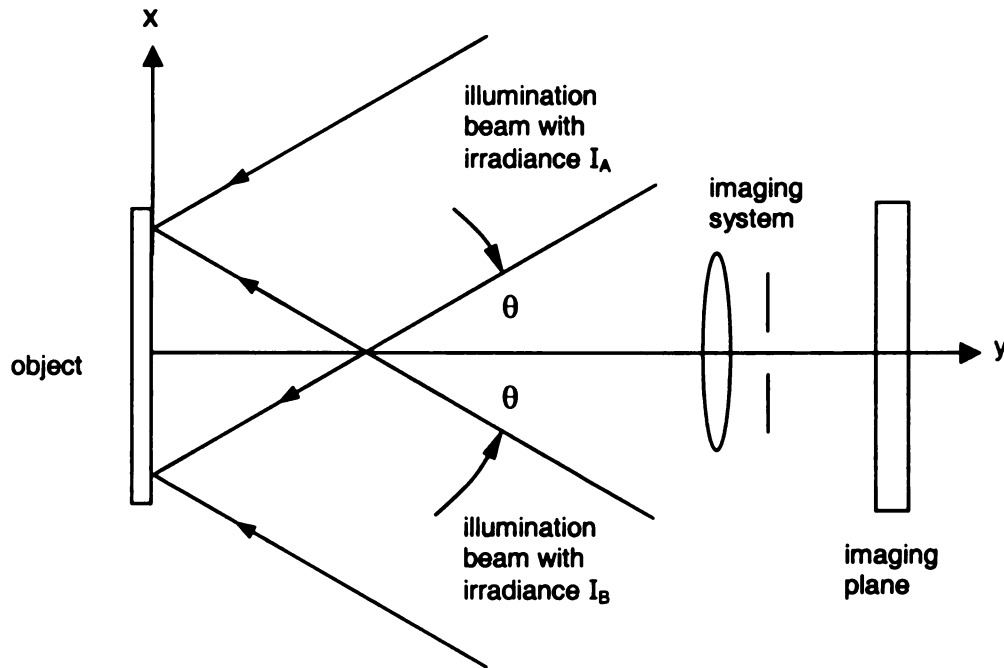


Figure 4.1 Simple in-plane speckle interferometer

Let $I_A(x,y)$ and $I_B(x,y)$ be the light irradiances of the first and second illumination beam, respectively, at the object plane. At any point the resultant irradiance from the combined beams can be written as

$$I_{before} = I_A + I_B + 2\sqrt{I_A I_B} \cos(\phi)$$

where I_A and I_B are the irradiances of two interfering beams, respectively, and ϕ is the phase difference between wave fronts. When the point is displaced by a vector u , the irradiance after deformation becomes:

$$I_{after} = I_A + I_B + 2\sqrt{I_A I_B} \cos(\phi + \Delta\phi)$$

where $\Delta\phi$ is a change of relative phase caused by motion.

The relationship between phase change $\Delta\phi$ caused by in-plane object displacement u_x at a point on the object surface is:

$$u(x, y) = \frac{\Delta\phi(x, y)\lambda}{4\pi \sin \theta}$$

where θ is the illumination angle from the object surface normal and λ is the wave length of light used.

4.1.4 IN-PLANE PHASE SHIFTING DSPI

Figure 4.2 shows a schematic of the in-plane dual-beam digital speckle interferometer used for this research, which has an angle of incidence $\theta = 21.8^\circ$. A beam splitter is used to obtain two coherent illumination beams by equally splitting light generated by the 7.7 mw HeNe Laser. Two microscope lenses expand the beams into a spherical wave front. The speckle irradiances are captured from the specimen with a CCD (charge-coupled device) camera and then sent to a computer to be processed. The camera is connected to a National Instruments IMAQ-1408 frame-grabber board that digitizes the analog video signal into a 512 x 512 x 8 bit pixel array.

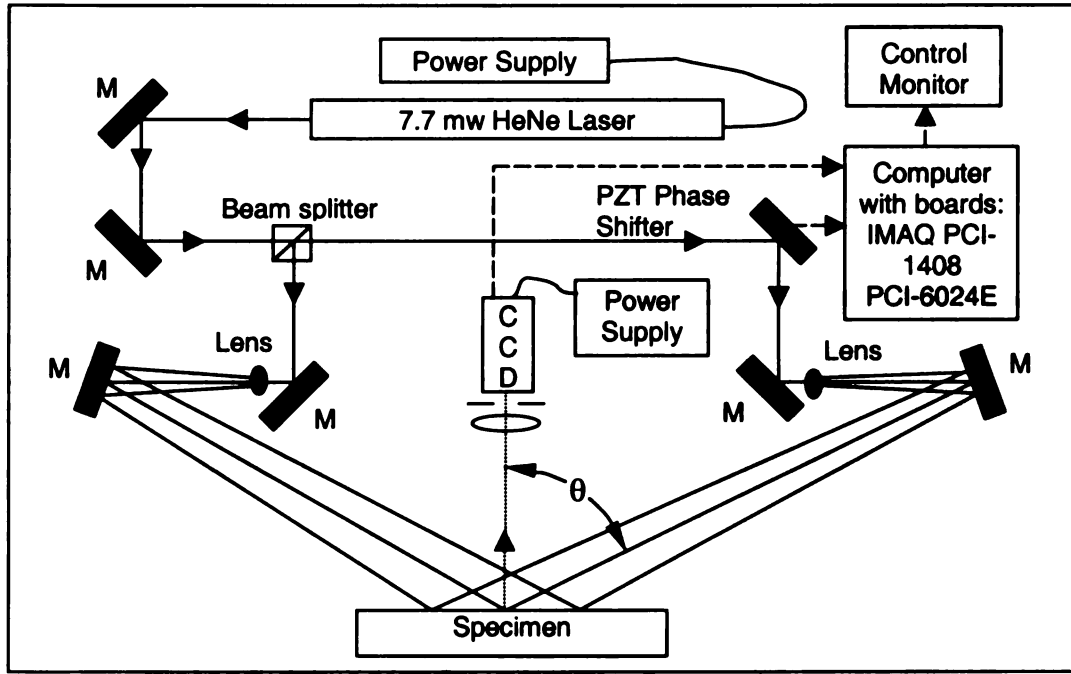


Figure 4.2 Dual-beam illumination setup of phase shifting ESPI

To interpret the speckle data quantitatively, a four-step phase-shifting technique is employed to quantitatively determine the phase change at each pixel. The phase shifting is implemented by a mirror mounted piezo-electric transducer (PZT), which is driven by a National Instruments PCI-6024 card. In a four-step, phase-shifting algorithm one of the object beams is shifted by 0 , $\pi/2$, π , and $3\pi/2$, while interference intensity data are digitized before and after object deformation. The phase difference at every pixel can be calculated by:

$$\phi(x, y) = \arctan \left(\frac{I_4(x, y) - I_2(x, y)}{I_1(x, y) - I_3(x, y)} \right)$$

where I_1 , I_2 , I_3 , and I_4 are the irradiances corresponding to phase shifts 0 , $\pi/2$, π , and $3\pi/2$ respectively.

Next, a phase difference map is determined from the phase maps obtained before and after deformation:

$$\Delta\phi(x, y) = \phi_{after}(x, y) - \phi_{before}(x, y)$$

The calculated phase value ϕ having modulo 2π from $-\pi$ to π is mapped into a 8-bit grayscale level image, giving a wrapped-phase map.

Next, the corresponding displacement map can be calculated from the sensitivity vector relation, where $\lambda=633\text{nm}$:

$$d_x = \lambda \frac{\Delta\phi}{2\pi} \cdot \frac{1}{2 \sin \theta}$$

4.1.5 STRAIN CALCULATION USING LOCAL PHASE-UNWRAPPING

There are several methods available to obtain the strain field; this research used a local phase-unwrapping technique developed by Hong (1997).

First, to provide a smoother map, a mean-method filter is used to remove some invalid pixels. In a 5 x 5 pixel window, two upper and lower thresholded values are chosen to count the number of upper-thresholded and lower-thresholded pixels. If there are more upper-thresholded pixels than lower-thresholded pixels, the later are unwrapped by adding 2π . Otherwise the upper-threshold pixels are unwrapped by subtracting 2π . Thus, the 2π phase discontinuity is eliminated through phase unwrapping.

A median filter is then used to further remove invalid pixels that still exist in the window and smooth the map, while preserving sharp 2π phase edges. Half

of the pixels in the window are chosen as a threshold. Invalid pixels then are counted. If there are more invalid pixels than the threshold, the center pixel in the window is replaced with the average of the phase values in the window. If not, the center pixel is marked as invalid.

Now the strain field can be determined by calculating the first spatial derivatives of the displacement map with respect to the x-axes. The least-square, surface-fitting method is used for the data smoothing and the approximate differentiation of discrete data. The least-square, surface fitting method finds a polynomial fitting function that minimizes the summation of squares of differences from the given data. The end result is an array of strain values that can be viewed on a spreadsheet or mapped into an 8-bit grayscale level image.

4.2 THE WASHER-NUT

Since a normal nut and washer covers the area of interest, an alternative fastener was developed. The new fastener had to perform the function of a normal washer and nut, but also be optically clear so that the area under the washer may be illuminated with the laser and captured with a CCD camera. These requirements led to the development of the 'washer-nut,' a circular bolt with the diameter of the washer manufactured from a thick transparent sheet material. Using a washer-nut, it may be possible to see how the amount of clamping force affects the strain field under the washer of the joint. It is expected that increasing the clamping force will decrease strain concentrations around the

bolt hole by increasing the load transferred through friction between the aluminum and composite plates.

Plexiglas was the first material considered for the washer-nut, however a Plexiglas nut cannot be torqued very tightly before fracturing because it is brittle. The next material considered was the transparent laminate developed for orthotropic photoelasticity test in Chapter 2; however, an orthotropic composite would not adequately model the mechanical properties of isotropic steel washer. Finally, LEXAN 9034 transparent polycarbonate sheet from GE Structured Products was considered and used as a material for the washer-nut.

LEXAN 9034 is a clear high-impact standard grade of polycarbonate sheet for general-purpose applications. The polycarbonate washer-nut can be made as stiff as a mild-steel washer using plate theory to solve for its thickness. According to plate theory, the stiffness of a washer can be modeled as

$$D = \frac{E(H)^3}{12(1 - \nu^2)}$$

where E = Flexural Modulus
 H = thickness
 ν = Poisson's Ratio

When the stiffness equations of 0.09" thick mild steel and polycarbonate are set equal to each other, the thickness of the polycarbonate washer may be solved for by using

$$\frac{29E6(.09)^3}{1 - 0.28^2} = \frac{0.345E6(H)^3}{1 - 0.38^2} \quad \text{Solving, } H=0.385"$$

LEXAN 9034 is available in 0.375" thick sheets. Accordingly, a washer-nut made of a 0.375" thick LEXAN 9034 polycarbonate is approximately as stiff as a mild-0.09" thick steel washer. Several sheets of 0.375" thick clear polycarbonate were obtained from GE Structured Products.

Manufacturing the washer-nut was simple; first a disc with the diameter of the washer was removed from a thick transparent sheet with a band saw and sanded to size on a disk sander. A 3/16" hole was then drilled through the center. Next, the washer-nut was threaded to match a 1/4"-20 shoulder bolt, with the tap mounted in a drill press as shown in Figure 4.3.

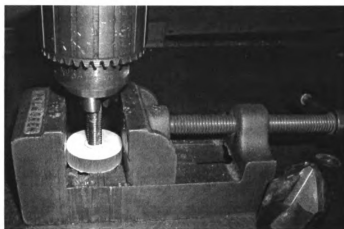


Figure 4.3 Threading of Washer-Nut

Washer-nuts made from this polycarbonate proved to fulfill all of the requirements as a transparent fastener. Ten washer-nuts were produced and tested to see how much torque could be applied before failure. To test the washer-nut, a torque wrench was used to apply torque while a pipe wrench held the washer-nut. All of the washer-nuts failed after they were torqued up 100-125 inch-pounds, which caused the washer-nut thread to strip. This research limited the torque applied to 40 inch-pounds to ensure a factor of safety of at least 2.

4.3 MANUFACTURE OF THE SPECIMEN

Scott Hodges[TARDEC] supplied the ½" thick quasi-orthotropic glass-reinforced-epoxy specimen studied in this research, which he manufactured in previous research work (Hodges 2000). The composite specimen was made from 54 plies of 18-oz S-2 plain weave fabric [0\90, 45\45]_s and Applied Poleramic SC-4 epoxy resin. To produce the specimen, Hodges first fabricated a 24" X 24" plate by means of Vacuum-Assisted Resin Transfer Molding (VARTM) and then cut it into 4" X 6" specimens with an OMAX 2652 JetMachining Center water-jet cutter. Next, Applied Composites Inc. professionally drilled a 0.5" nominal size hole in order to minimize fiber damage and ply delamination. The specimen has the same dimensions as the photoelastic specimen made in Chapter 3. Unfortunately, mechanical properties of the laminate have not been determined.

The aluminum plate and shoulder bolt were the same as were used in the photoelastic analysis of Chapter 3. Since the bolt blocked part of the illumination beams, the thread was trimmed to the thickness of the washer-nut.

4.4 EXPERIMENTAL SETUP

Figure 4.4 shows the Measurements Group Photoelastic Division Model 162 screw-operated loading frame used to deform the single-lap, single-bolted joint. This horizontal extension loading system was a rigid structure that could provide constant deformation of the joint. It was imperative for the load frame to

be as rigid as possible to minimize rigid body deformations. The composite specimen was clamped between two 1" wide steel beams, which were secured with a bolt through both ends; a C-clamp was also fastened in the middle of the beams. The specimen fixture was then clamped to the load frame between two 1" wide steel beams along with C-clamps on either side of the specimen. The aluminum side of the joint was bolted to the screw system. Both the load frame and DSPI unit were mounted on a Model 76-455-02 vibration-insulated optical table from Technical Manufacturing Company.

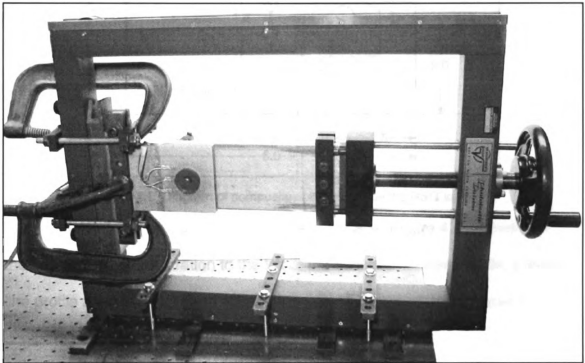


Figure 4.4 Loading system for DSPI analysis

The area around the bolt hole of the specimen was lightly coated with Metallic Finish Lacquer to help generate a fully developed speckle pattern (Cloud 1995).

The system was initially tested with a pin connection over a large area seen in Figure 4.5 to determine the region of interest where the high strain concentration will occur. Also, to verify the strain field computed by DSPI, three Micro-Measurement EA-13-120LZ-120 strain gages were mounted on the specimen as shown in Figure 4.5.

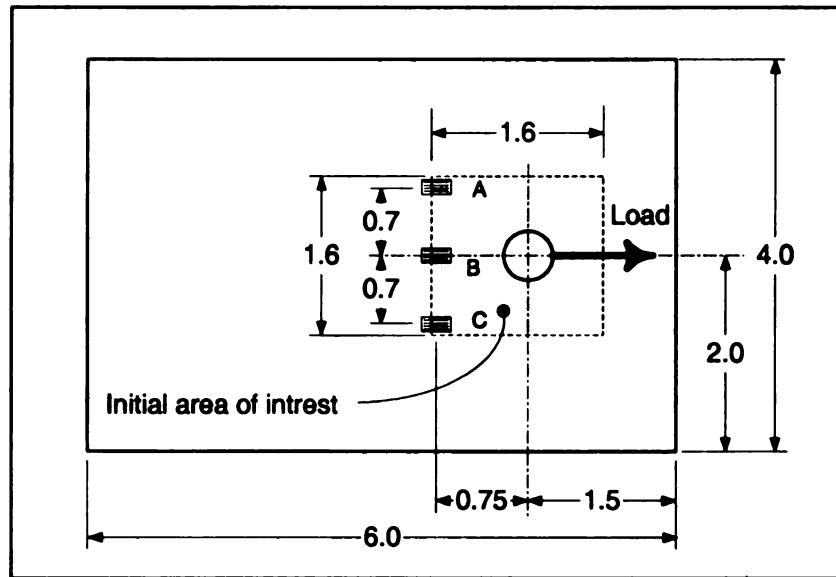


Figure 4.5 Diagram of composite specimen showing RSG locations

The phase map from the initial area of interest, Figure 4.6, shows that there is a strain concentration to the left of the bolthole. Consequently, a strain line profile as shown in Figure 4.7 was acquired for each clamping case to compare strain distributions.



Figure 4.6 Phase map of initial area of interest for pin connection

For the bolted connection, the area of interest as shown in Figure 4.7 was limited to the area under the washer-nut. The intensity captured by the camera in the washer-nut area was significantly less than the area outside. Therefore, a larger aperture was necessary to get adequate intensity levels when analyzing areas within the washer-nut.

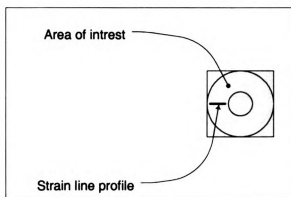


Figure 4.7 Area of interest and strain line profile under washer-nut

4.5 EXPERIMENTAL PROCEDURE

The joint was pre-loaded in tension to reduce rigid body deformations. It was possible to maintain a consistent pre-load for each test by keeping the load

screw at the same rotation at the start of the experiment, although the exact amount of pre-load is unknown.

A LabVIEW (National Instruments Corp.) program, developed by Xu Ding, controlled the CCD camera and PZT and performed the digital-signal processing. To obtain the strain field, the phase map before deformation was computed first. Next, the load was applied by rotating the screw $1/8^{\text{th}}$ of a turn. Subsequently, the phase map after deformation was computed. The deformed phase map was then subtracted from the un-deformed phase map to create a phase change map and smoothed with median filters. After that, the strain map was calculated with a local phase-unwrapping algorithm and least-square, surface-fitting algorithm developed by Hong (1997). A strain line profile was then extracted from the strain field array. Lastly, in order to compare the strain line profiles of each clamping case, they were normalized by dividing by the strain at Gage B after deformation.

4.6 RESULTS

The DSPI and RSG strain results for the pin connection are compared in Table 4.1. These results give confidence in the DSPI strain field, since there is a good correlation between DSPI and RSG strains.

	Gage A	Gage B	Gage C
DSPI strain ($\mu\epsilon$)	-37	-8	-32
RSG strain ($\mu\epsilon$)	-37	-5	-35

Table 4.1 DSPI vs. RSG strain on pin connection

The DSPI phase change and strain map results for the four clamping cases are shown in Figure 4.8. It can be seen that increasing the clamping force significantly changes the strain field.

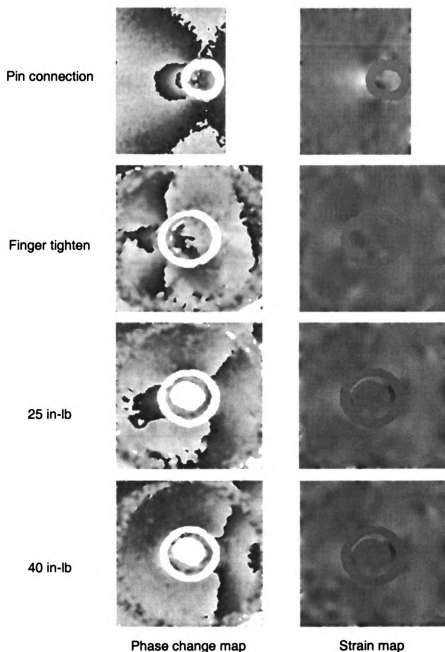


Figure 4.8 DSPI phase change and strain map results

A large strain concentration to the left of the bolthole due to tilting of the bolt can be seen in the pin connection. This concentration was considerably reduced even with a finger-tightened, washer-nut. Torquing the washer-nut to 25in-lb and then 40in-lb further reduces the strain concentration to the left of the bolthole.

The DSPI normalized strain line profile for each clamping case is shown in Figure 4.9.

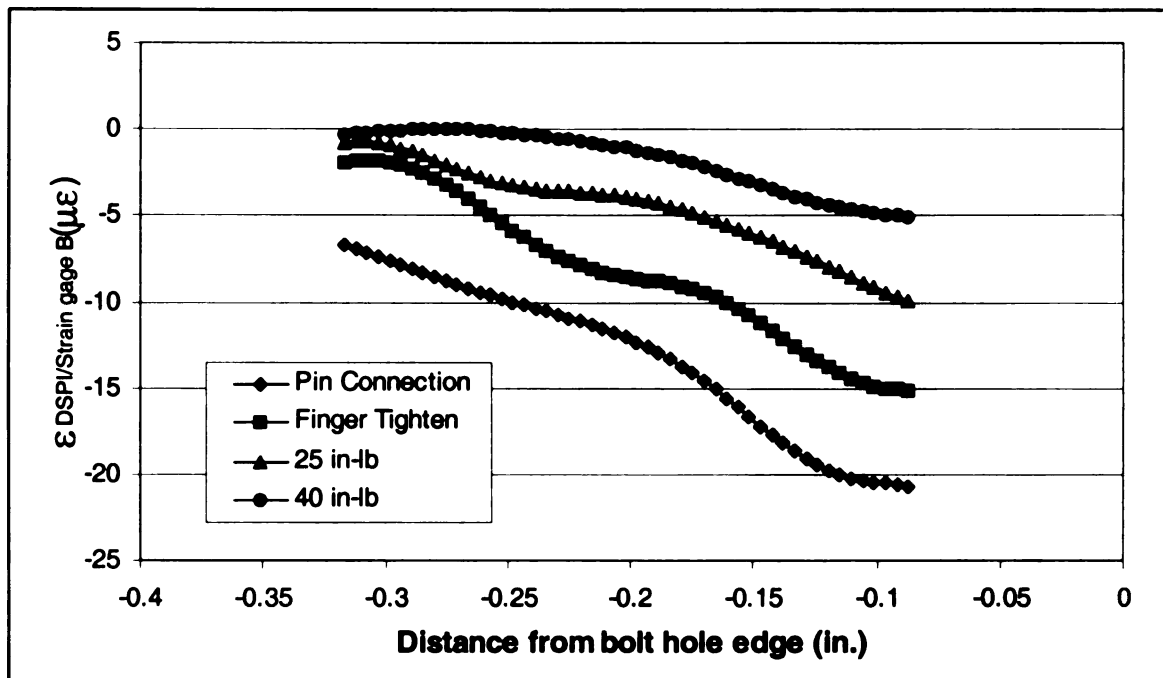


Figure 4.9 DSPI normalized strain line profile

The strain gradients were not as high as expected near the bolthole edge, which may be explained in part by either the effect of friction and bolt/bolthole interface or mathematical approximations affecting strain calculations near the edges of inadequate illumination (Hong 1997).

In any case, the normalized strain line profiles further illustrate that increasing the bolt torque reduces strain concentrations near the bolthole edge.

This pattern was as expected because the clamping of a tightened bolt causes a considerable part of the applied load to be transferred by friction between components, thereby reducing stress concentrations at the hole-edge interface.

CHAPTER 5 – CONCLUSIONS AND RECOMMENDATIONS

This thesis is part of a larger effort to research the strength of a single-lap, single-bolt joint between a thick polymer matrix composite (PMC) and aluminum section that is representative of those to be employed on ARMY heavy-duty land vehicles. Poorly designed joints significantly detract from the weight advantages of composites over metals, which can lead to either overweight or defective structures. There has been little published research on the single lap bolted joint, owing to the difficulty of analyzing this configuration. The goal of this thesis was to contribute to the development of two experimental methods to analyze the stress distribution near the region around the bolt hole; then acquire results from those techniques to complement and verify the FEM stress predictions.

The first method was an embedded polariscope orthotropic photoelastic stress analysis to study the contact stress distribution in the bearing plane of the composite between the bolt and bolthole. In order to model composite orthotropic behavior, a transparent birefringent orthotropic material was developed and characterized.

The reinforcement selected was a plain weave E-glass fabric style 3733 with S-910 finish manufactured by J.P. Stevens, which had worked well for previous two-dimensional orthotropic photoelastic research. However, the Marblette 658/558 epoxy resin used in those studies is no longer available. Therefore, sixteen epoxies were obtained, and numerous composite samples were fabricated and tested for their transparency and birefringence. Epoxies,

Etc... 20-3302 Optically Transparent Epoxy proved to be the optimal matrix material for the E-glass fibers chosen. With composite samples of 20-3302 resin and E-glass, it was possible to read fine print through 0.3" of the composite material, and generate five sharp fringes edgewise through a 0.1" wide, 0.3" thick specimen in four-point bending. Incidentally, the 20-3302 resin might not work as well with other E-glass because there is a broad range of glass compositions that meet the definition of E-glass, and different compositions will have different refractive indices and bonding characteristics.

The key factors to fabricating a transparent composite were:

- Matching the refractive indices of the matrix and glass**
- A resin with a long cure time and pot life to help minimize thermal induced stresses and initial birefringence**
- Removal of entrapped air using a roller during lay-up**
- A low viscosity resin to facilitate wetting and air removal**
- Proper wet-out of fibers by subjecting the composite to a vacuum for an hour, and having good fiber-matrix compatibility**

The major limiting factors in producing an optically clear composite were:

- E-glass fabric is not manufactured to be optically transparent**
- E-glass fabric glass is not manufactured to have a reliable refractive index**

Figure 5.1 defines the composite plate coordinate system used throughout this thesis.

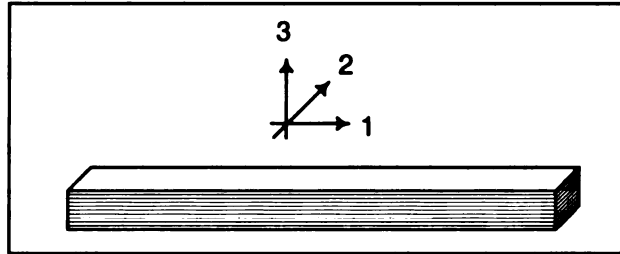


Figure 5.1 Coordinate system

Several tensile specimens were produced to determine the photoelastic constants. The stress-optic coefficient, F_3 was determined utilizing the Tardy method of goniometric compensation. The specimen was loaded from 0 to 450 lbs. and generated a maximum of 2.75 fringes. F_3 was established to be 504.2 psi-in./fringe. F_2 was determined by direct observation of whole and half order fringes with a specimen. The Tardy method of goniometric compensation was not used because the laminate is significantly less transparent in Direction 2, and the background brightness varied as the polarizer rotated, which made determination of fringe order very difficult. The specimen was loaded from 0 to 350 lbs. and generated a maximum of 3.5 fringes. F_2 was found to be 415.3 psi-in./fringe.

The material combination found in this research is comparable to the material used in numerous other orthotropic photoelasticity studies, which had similar stress-optic coefficients, and were able to generate adequate fringe patterns for two-dimensional analysis. Although several studies (Prabhakaran 1982 and Hyer and Liu 1985) used two-dimensional orthotropic photoelasticity to

study the stresses in pin-loaded PMC plates, in plates as thick as the one currently studied, the stresses will vary through the thickness. Accordingly, it was necessary to perform a three-dimensional stress analysis to analyze photoelastic fringes through the edge of the composite. Only one study (Chandrashekhara et al. 1977) has been published on three-dimensional orthotropic photoelasticity, and they applied the stress freezing technique to low fiber-volume specimens.

Employing an embedded polariscope in the transparent composite specimen did not prove to be as useful as expected. Although the results showed that increasing the clamping force decreased stress concentrations, little if any quantitative data may be obtained from the fringe patterns because they had poor contrast. 25 in-lb bolt torque applied to the bolt initially generated a fairly distinct horizontal fringe, which would equate to 2517 ± 1258 PSI. However, immediately after clamping, the fringe expanded over time toward the bolt under the washer. When 80 lb. was applied to the joint having pin connection, two vague fringes were produced, which would equate to 5034 ± 1258 PSI. However the fringes were not sharp enough to tell for certain if they were in fact two distinct fringes. It is not known why the specimen with the embedded polariscope did not generate good fringes, while a monolithic piece could.

Even if this study generated distinct fringe patterns, it is not known how useful they would be, as the stress distribution of the embedded polariscope will disrupt the orthotropic behavior of the composite specimen. Also, it is difficult to

determine the validity of the fringe patterns, as there is little if anything to compare these results to. In addition, the bolt could not sustain more than 25 in-lbs of bolt torque, and/or more than 80 lbs of applied load to the joint before failure because of insufficient bonding shear strength at the embedded polariscope. The type of joint studied is likely to be torqued to 75 - 100 ft-lbs, and see 10,000-20,000 lbs of load in service (Hodges 2000).

The implications of the orthotropic photoelasticity material time effect as discussed in section 3.5 are not known. If in fact the relaxation of birefringence in the composite is related to a relief of stress in the epoxy matrix, the material could be used to study the effect of large impacts that ARMY heavy-duty, land vehicles could expect to see. However, it is not known if this phenomenon occurs only in the photoelastic material developed in this research or if it is common to opaque composites used in structural applications. Although the 20-3302 resin is designed for glass or plastic applications requiring outstanding adhesion, it is not typically used as a matrix in fiber-reinforced composites.

The second experimental method was a Digital Speckle Pattern Interferometry (DSPI) surface strain analysis of the single-lap, bolted joint between composite and aluminum. Since a normal nut and washer covers the area of interest, an optically clear polycarbonate washer-nut was developed so that the area under the washer may be illuminated with the laser and captured with a CCD camera. This washer-nut made it possible to study how increasing the clamping force affects the strain field under the washer of the joint.

The DSPI strain map of the pin connection showed a large strain concentration to the left of the bolthole due to tilting of the bolt. This concentration was considerably reduced even with a finger-tightened, washer-nut. Torquing the washer-nut to 25in-lb and then 40in-lb further reduced the strain concentration on the bolthole. It was also found that the strain at an area 0.1in from the bolthole was reduced by approximately 80% by torquing the washer-nut to 25in-lb. It was not possible to analyze areas closer to the bolthole edge because the thick washer-nut blocked some of the DSPI beams, which illuminated the specimen at an angle.

To verify the strain field computed by DSPI, three strain gages were mounted on the specimen. There was good correlation between DSPI and RSG strains, which gave confidence in the DSPI stain field. However, the gages were not mounted under the washer-nut, consequently it is not known how the washer-nut affected the DSPI results. Several factors may have produced significant error in the results. One possible error is that the refractive index changes as the laser beam passes through the washer-nut, which would bend the illumination beam. Another issue is that polycarbonate is moderately birefringent. As load is applied to the joint, resultant forces will vary over the washer-nut. So the stress-induced birefringence of the washer-nut may not only affect the results, but also affect them differently over the area.

Overall, the DSPI and photoelasticity results demonstrate that increasing bolt torque significantly decreases stress concentrations, which correlate well

with phenomenological mechanical tests (Hodges 2000) that demonstrated the potential to improve joint strength by bolt torque.

Possible future research areas are:

- Improve the transparency of the orthotropic photoelastic material with the use of either fiber-optic cables or optical grade glass, which is crucial if fringe quality is to be improved. An orthotropic material with improved transparency would also allow larger orthotropic models to be produced.
- Further research the time effect of the orthotropic photoelastic material as discussed in section 3.5.
- Increase or decrease the stress-optic coefficient of the orthotropic photoelastic material as needed to analyze the joint at different loads.
- Increase the allowable load on the joint with the embedded polariscope by either improving its design or the bond strength between composite specimen, polarizer, analyzer, $\lambda/4$ wave plates, and polycarbonate or other joint material used.
- Employ an embedded polariscope in the opposite side of the bolthole where DSPI results show a strain concentration in pin connection.
- For DSPI analysis, develop a stiffer transparent material to decrease the thickness of the washer-nut. A thinner washer-nut would increase the possible area of interest in DSPI analysis since it is illuminated at an angle, and would reduce whatever effects that may be caused by

birefringence of the washer-nut as well as the change in refractive index of the material that the laser illumination passes through. In addition, increase the toughness of the material used for the washer-nut, which would allow increased amounts of torque. It would be ideal to be able to analyze the strain field underneath a bolt that is loaded as in service conditions.

- Use the washer-nut with DSPI to further study the effects of varying clamping torque, as well as washer size and clearance between bolt and hole. Also, a more rigid load system capable of much higher loads would allow the study of in-service, heavy-loading conditions of the joint.

LIST OF REFERENCES

LIST OF REFERENCES

- Agarwal, B.D., and Chaturvedi, S.K. (1978). "Development and Characterisation of Optically Superior Photoelastic Composite Materials," *International Journal of Mechanical Sciences*, 20, 407-414.
- Allen, S. (2002) Personal contact, E-mail, September 25, 2002. Advanced Glassfiber Yarns LLC., WHQ, 2558 Wagener Road, Aiken SC 29802
- Askadskii A., Marshalkovich A., Goleneva L., et al. (1987). "Optical And Mechanical Properties Of Polymeric Materials, Intended For The Modeling Of The Stresses And Deformed State Of Composite Constructions By The Photoelasticity Method," *Mechanics of Composite Materials*, 23 (2), 252-257.
- Chandrasekhara, K., Jacob, K.A., and Prabhakaran, R. (1977). "Towards Stress-Freezing in Orthotropic Model Materials," *Experimental Mechanics*, 17, 317-320.
- Chaturvedi, S.K. (1982). "Fundamental Concepts Of Photoelasticity For Anisotropic Composite Materials," *International Journal of Engineering Sciences*, 20 (1), 145-157.
- Cooper, C. and Turvey, G.J. (1995). "Effects of Joint Geometry and Bolt Torque On the Structural Performance of Single Bolt Tension Joints In Pultruded GRP sheet material," *Composite Structures*, 32, 217-226.
- Cloud, G.L. (1995). Optical Methods of Engineering Analysis. New York: Cambridge University Press.
- Dally, J.W., and Riley, W.F. (1967). "Initial Studies in Three-Dimensional Dynamic Photoelasticity," *Journal of Applied Mechanics*, 34 (2), 405-410.
- Dally, J.W. and Prabhakaran, R. (1971). "Photo-orthotropic-elasticity," *Experimental Mechanics*, 11 (8), 346-356.
- Daniel I.M., Koller G.M., and Niiro, T. (1984). "Development And Characterization Of Orthotropic-Birefringent Materials," *Experimental Mechanics*, 24 (2), 135-143.
- Daniel, I.M., Niiro, T. and Koller, G.M. (1981). "Development Of Orthotropic Birefringement Materials For Photoelastic Stress Analysis," NASA Contract Report 165709, 10-18.
- Doyle, J.F. and Hyer, M.W. (1985). "Optical Characterization of a Photo-Orthotropic Material," *International Journal Of Mechanical Sciences*, 27 (11/12), 697-702.
- Fanderlik, I. (1983). *Optical Properties of Glass*. New York: Elsevier Science Publishers.

Grakh and Mozhanskaya, (1971). "Type of Mechanically Anisotropic Optically Sensitive Material," *Mekhanika Polimerov*, 5, 835-839. (Written in Russian)

Hayashi, T. (1962). "Photoelastic Method of Experimentation for Stress Analysis on Orthotropic Structures," *Proceedings of the Fourth International Symposium on Space Technology and Science*, Tokyo, 156-169.

Herrera-Franco, P.J. and Cloud, G.L. (1992). "Strain-Relief for Composite Fasteners – An Experimental Study," *Journal of Composite Materials*, 26 (5), 751-768.

Hodges, S.E. (2000). A Study of Bolted Single Lap Joints Between Composites and Aluminum, M.S. Thesis, Michigan State University.

Hong, S. (1997). Digital Image Processing Algorithms For Electronic Speckle Pattern Interferometry, M.S. Thesis, Michigan State University.

Horridge, G.A. (1955). "A Polarized Light Study of Glass Fibre Laminates," *British Journal of Applied Physics*, 6, 314-319.

Hyer, M.W. and Liu, D. (1985). "Stresses in Pin-Loaded Orthotropic Plates: Photoelastic Results," *J. Composite Materials*, 19 (2), 138-153.

Ireman, T., Ranvik, T., and Eriksson, I. (2000). "On Damage Development in Mechanically Fastened Composite Laminates," *Composite Structures*, 49, 151-171.

Jones, R. and Wykes, C. (1989). Holographic and Speckle Interferometry, 2nd edition: Cambridge University Press.

Kang, S., Lin, H., Day, D., and Stoffer, J. (1997). "Optically Transparent Polymethyl Methacrylate Composites Made with Glass Fibers of Varying Refractive Index," *Journal of Materials Research*, 12 (4), 1091-1001.

Lanza Di Scalea, F. (1996). Phase-Stepped Digital Speckle Pattern Interferometry (DSPI) and its Application to Mechanical Joining of Composite Materials, M.S. Thesis, Michigan State University.

Lanza di Scalea F.L., Hong S.S., and Cloud G.L. (1998). "Whole-Field Strain Measurement In a Pin-Loaded Plate By Electronic Speckle Pattern Interferometry And The Finite Element Method." *Experimental Mechanics*, 38 (1), 55-60.

Liu, D. (1990). "Photoelastic Study on Composite Stitching," *Experimental Techniques*, 14 (1), 25-27.

- Loewenstein, K. L. (1993). The Manufacturing Technology of Continuous Glass Fibers. New York: Elsevier Science Publishers.
- Lu, C.K., Chen, J.C., and Lin, C.H. (1993). "Stresses Of Plain Fabric Composites Containing Pin-Loaded Holes," *Sampe Journal*, 29 (4), 16-25.
- Olson, J.R., Delbert, D.E., and Stoffer, J.O. (1992). "Fabrication and Mechanical Properties of an Optically Transparent Glass Fiber/Polymer Matrix Composite," *Journal Of Composite Materials*, 26 (8), 1181-1193.
- Papirino, R., and Becker. H. (1966). "A Bonded Polariscopes for Three-Dimensional Photoviscoelastic Studies," *Experimental Mechanics*, 6 (12), 609-616.
- Pih, H. and Knight, C. E. (1969). "Photoelastic Analysis of Anisotropic Fiber Reinforced Composites," *Journal Of Composite Materials*, 3, 94-107.
- Pipes, R.B. and Dalley, J.W. (1973). "On the Fiber-reinforced Birefringent Composite Materials," *Experimental Mechanics*, 13 (8), 348-349.
- Pipes, R.B. and Rose, J.L. (1974). "Strain Optic Law for a Certain Class of Birefringent Composites," *Experimental Mechanics*, 14 (9), 355-360.
- Prabhakaran, R. (1980). "Fabrication of Birefringent Anisotropic Model Materials," *Experimental Mechanics*, 20 (9), 320-321.
- Prabhakaran, R. (1982). "Photoelastic Investigation of Bolted Joints In Composites," *Composites*, 13 (3), 253-256.
- Ramesh, K. and Tiwari, N. (1993). "A Brief Review of Photo-Orthotropic Elasticity Theories," *Sadhana-Academy Proceedings in Engineering Sciences*, 18: Part 6, 985-997.
- Ravi, S. (1998). "Development of Transparent Composite For Photoelastic Studies," *Advanced Composite Materials*, 7 (1), 73-81.
- Ravi S., Iyengar N., Kishore N., and Shukla A. (2001). "Experimental studies on damage growth in composites under dynamic loads," *Applied Composite Materials*, 8 (2), 79-97.
- Rispler, A.R., Steven, G.P., and Tong, L.Y. (2000). "Photoelastic Evaluation Of Metallic Inserts Of Optimised Shape," *Composites Science And Technology*, 60 (1), 95-106.
- Sampson, R.C. (1970). "A Stress-Optic Law for Photoelastic Analysis of Orthotropic Composites," *Experimental Mechanics*, 10 (5), 210-215.

Serabian, S.M. and Anastasi, R.F. (1991). "Out-of-Plane Deflections of Metallic and Composite Pin-Loaded Coupons," *Experimental Mechanics*, 31 (1), 25-32.

Tranmposch, H., and Gerard, G. (1961). "Exploratory Studies in Three-Dimensional Photo-Thermoelasticity," *Journal of Applied Mechanics*, 28 (1), 35-40.

van Zanten, J.H., Wallace, W.E., and Wu, W.L. (1996). "Effect of Strongly Favorable Substrate Interactions on the Thermal Properties of Ultrathin Polymer Films," *Physical Review E*, 53 (3), R2053–R2056.

Zhang, W. and Wang, Y. (1995). "The Photoelastic Behavior Of Optically Heterogeneous Fiber Composites - 1. The Equivalence Of Birefringence In Optically Heterogeneous Unidirectional Fiber Composites," *International Journal Of Mechanical Sciences*, 37 (9), 919-931.

Zhang, W. and Wang, Y. (1995). "Photoelastic Behavior Of Optically Heterogeneous Fiber Composites - 2. The Principal Direction Of The Equivalent Birefringence For Optically Heterogeneous Unidirectional Fiber Composites," *International Journal Of Mechanical Sciences*, 37 (9), 933-942.

MICHIGAN STATE UNIVERSITY LIBRARIES



3 1293 02470 0340